Myotubularin related protein-2 and its phospholipid substrate PIP_2 control Piezo2-mediated mechanotransduction in peripheral sensory neurons

Pratibha Narayanan[1], Meike Huette[1], Galina Kudryasheva[2], Francisco J Taberner[3], Stefan G. Lechner[3], Florian Rehfeldt[2], David Gomez-Varela[1], Manuela Schmidt[1]*

[1] Emmy Noether-Group Somatosensory Signaling and Systems Biology, Max Planck Institute for Experimental Medicine, 37075 Goettingen, Germany; [2] University of Goettingen, 3rd Institute of Physics - Biophysics, 37077 Goettingen, Germany; [3] Institute of Pharmacology, 69120 Heidelberg, Germany

*Corresponding author: Manuela Schmidt; Max-Planck Institute for Experimental Medicine. Somatosensory Signaling and Systems Biology Group. D-37075, Goettingen, Germany; mschmidt@em.mpg.de

Acknowledgements: The authors would like to thank Ardem Patapoutian (HHMI, TSRI, La Jolla) for kindly providing Piezo2^{GFP} mice and *Piezo* plasmids, Walter Stühmer and Luis Pardo (both MPI for Experimental Medicine, Goettingen) for generously providing the electrophysiology equipment, and Kathrin Willig and Joris van Dort for preliminary experiments. Many thanks to Sergej Zeiter (MPI for Experimental Medicine, Goettingen) for excellent technical assistance. We are grateful to Ardem Patapoutian, Viktor Lukacs and Luis Pardo for thoughtful comments on the study and manuscript. This work was supported by the Emmy Noether-Program of the Deutsche Forschungsgemeinschaft (DFG) (SCHM 2533/2-1 to M.S.), the DFG Collaborative Research Center 889 (project A9 to M.S.), a DFG research grant (DFG GO 2481/2-1 to D.G.V.), the Max Planck Society and GGNB PhD fellowships (to P.N. and M.H.). The authors declare no competing financial interest.

Abstract

Piezo2 ion channels are critical determinants of the sense of light touch in vertebrates. Yet, their regulation is only incompletely understood. We recently identified myotubularin related protein-2 (Mtmr2), a phosphoinositide (PI) phosphatase, in the native Piezo2 interactome of murine dorsal root ganglia (DRG). Here, we demonstrate that Mtmr2 attenuates Piezo2-mediated rapidly adapting mechanically activated (RA-MA) currents. Interestingly, heterologous Piezo1 and other known MA current subtypes in DRG appeared largely unaffected by Mtmr2. Experiments with catalytically inactive Mtmr2, pharmacological blockers of $PI(3,5)P_2$ synthesis, and osmotic stress suggest that Mtmr2-dependent Piezo2 inhibition involves depletion of $PI(3,5)P_2$. Further, we identified a $PI(3,5)P_2$ binding region in Piezo2, but not Piezo1, that confers sensitivity to Mtmr2 as indicated by functional analysis of a domain-swapped Piezo2 mutant. Altogether, our results propose local $PI(3,5)P_2$ modulation via Mtmr2 in the vicinity of Piezo2 as a novel mechanism to dynamically control Piezo2-dependent mechanotransduction in peripheral sensory neurons.

Introduction

Our sense of touch relies on mechanotransduction, i.e. the conversion of mechanical stimuli to electrical signals in primary afferent sensory neurons of the somatosensory system. Piezo2 ion channels have emerged as major somatosensory mechanotransducers and mediate rapidly adapting

mechanically activated (RA-MA) currents in sensory neurons, such as those of dorsal root ganglia (DRG) (Coste et al., 2010; Coste et al., 2012). By now it has been established that Piezo2 is crucially involved in vertebrate light touch and proprioception (Coste et al., 2010; Coste et al., 2012; Florez-Paz et al., 2016; Ranade et al., 2014; Woo et al., 2015; Woo et al., 2014). Despite its importance, the regulation of native Piezo2 is only beginning to be elucidated. Mechanistically, several scenarios might be at play (Wu et al., 2016b): direct action of phospholipids, the modulation of local membrane properties and protein-protein interactions, just to name a few. Studies on other mechanosensitive ion channels such as the family of small conductance channels (MscS) (Sukharev, 2002) as well as eukaryotic TRAAK, TREK1 (Brohawn et al., 2014a; Brohawn et al., 2014b) and Piezo1 (Cox et al., 2016; Lewis and Grandl, 2015; Wu et al., 2016a) demonstrated their direct interplay with components of the lipid bilayer. In case of Piezo2, RA-MA currents were shown to be inhibited through depletion of phosphatidylinositol 4,5-bisphosphate ($PI(4,5)P_2$) and phosphatidylinositol 4-monophosphate (PI(4)P) (Borbiro et al., 2015), and also by depletion of cholesterol at the plasma membrane (Qi et al., 2015). Besides, lipid- or cytoskeleton-induced changes in plasma membrane tension have been shown to impact somatosensory mechanotransduction (Jia et al., 2016; Morley et al., 2016; Qi et al., 2015). In contrast to the vast knowledge of the molecular network governing mechanotransduction in the nematode C. elegans, to date only few protein-protein interactions relevant for Piezo2 physiology have been identified in vertebrates. These include stomatin-like protein STOML3 (Poole et al., 2014; Qi et al., 2015; Wetzel et al., 2007), unidentified protein tethers to the extracellular matrix (Hu et al., 2010) and Pericentrin (Narayanan et al., 2016). It is noteworthy that all of these exhibit pronounced effects on the magnitude or mechanical sensitivity of Piezo2 RA-MA currents.

In order to advance the molecular understanding of Piezo2 regulation, we recently performed an interactomics screen, which revealed several additional binding partners of native Piezo2 in murine DRG (Narayanan et al., 2016). A significantly enriched and prominent member of the Piezo2 interactome was myotubularin related protein 2 (Mtmr2) (Narayanan et al., 2016), a phosphoinositide phosphatase of the MTMR family (Bolino et al., 2002). Interestingly, Mtmr2 was previously described to be highly expressed in DRG sensory neurons and Schwann cells (Bolino et al., 2002). Functionally, Mtmr2 catalyzes the removal of a 3-phosphate group from its phosphoinositide (PIPs) substrates phosphatidylinositol 3-monophosphate PI(3)P and phosphatidylinositol 3,5-bisphosphate $PI(3,5)P_2$ (Begley et al., 2006; Berger et al., 2002). Remarkably, $PI(3,5)P_2$ is much less abundant than most other PIPs, e.g. $PI(4,5)P_2$ (Zolov et al., 2012), but can be rapidly and transiently regulated by a large enzymatic protein complex in response to cellular stimulation (McCartney et al., 2014a; Vaccari et al., 2011; Zolov et al., 2012). Hence, $PI(3,5)P_2$ is exquisitely suited to control rapid cellular signaling events (Ho et al., 2012; Ikonomov et al., 2007; Li et al., 2013a; McCartney et al., 2014a; Zhang et al., 2012), and also the activity of receptors and ion channels (Dong et al., 2010; Ho et al., 2012; Klaus et al., 2009; McCartney et al., 2014a; McCartney et al., 2014b; Tsuruta et al., 2009). Altogether, this raises the question whether Mtmr2 and its PIP substrates are implicated in Piezo2-mediated mechanotransduction and generally, in somatosensory mechanosensation.

Here, we show that Mtmr2 levels control Piezo2-mediated RA-MA currents. While elevated Mtmr2 expression attenuated Piezo2 RA-MA currents, siRNA-mediated knockdown of Mtmr2 resulted in Piezo2 RA-MA current potentiation. Interestingly, heterologously expressed Piezo1 and other known subtypes of MA currents in DRG were largely unaffected. Mechanistically, our experiments with catalytically inactive Mtmr2, pharmacological inhibitors, and osmotic stress suggest that changes in

the levels of $PI(3,5)P_2$ regulate Piezo2 RA-MA currents. In line with these findings we uncovered a previously unknown polybasic motif in Piezo2 that can bind $PI(3,5)P_2$ and confers Piezo2 sensitivity to Mtmr2. Collectively, our study reveals a link between Mtmr2 activity and $PI(3,5)P_2$ availability to locally control Piezo2 function.

Results

Mtmr2 suppresses Piezo2-mediated RA-MA currents

Our previous work revealed Mtmr2 as a highly enriched member of the native Piezo2 interactome in DRG (significance of identification: $p = 0.00030$, unpaired t-test; enrichment factor: $\log_2$ 9.96) (Narayanan et al., 2016). We first validated the reported expression of Mtmr2 in peripheral sensory neurons of DRG (Previtali et al., 2003; Vaccari et al., 2011) including those neurons expressing Piezo2 (Figure 1-figure supplement 1a,b). For a more detailed subcellular analysis we used the proximity ligation assay (PLA). In this way we could show the close vicinity of Piezo2 and Mtmr2 in both, somata and neurites of cultured DRG neurons, and upon co-transfection in HEK293 cells (Figure 1a-d and Figure 1-figure supplement 1c,d). It is important to note here that the PLA technique is prone to high background upon heterologous expression as shown by our additional control experiments in HEK293 cells (Figure 1-figure supplement 1d). In these we co-overexpressed Piezo2 with TRPA1 and Vti1b, respectively. Both of these controls exhibited clear PLA signal (likely attributable to massive overexpression upon transfection), though less than co-overexpression with Mtmr2 (Figure 1-figure supplement 1d).

Following, we wanted to assess whether Mtmr2 affects Piezo2 function. To this end we performed electrophysiological measurements of Piezo2-mediated RA-MA currents in HEK293 cells, which represent a well-defined heterologous system to study Piezo2 function (Coste et al., 2010; Poole et al., 2014). Interestingly, Mtmr2 co-expression led to a pronounced reduction of Piezo2-mediated RA-MA currents compared to mock conditions (Figure 1e,f). Moreover, the displacement threshold of RA-MA currents was significantly increased upon Mtmr2 overexpression indicating the requirement of stronger mechanical stimulation to reach a threshold current amplitude (Supplementary File 1; please see Methods for details on the calculation of the displacement threshold) (Eijkelkamp et al., 2013; Morley et al., 2016; Narayanan et al., 2016). Importantly, the inactivation time constant of Piezo2 currents remained unchanged upon Mtmr2 co-expression (Supplementary File 1). These data indicate that Mtmr2 overexpression suppresses Piezo2 currents in HEK293 cells while maintaining their defining property, i.e. rapid adaptation. To exclude that Mtmr2 overexpression renders cells unhealthy and might therefore unspecifically suppress Piezo2 currents, we co-expressed Mtmr2 with Kv1.1 and measured voltage-gated currents, which were similar to mock transfected controls (Figure 1-figure supplement 2a). In addition, we asked whether Mtmr2 may modulate MA currents generated by Piezo1, the homologue of Piezo2 (Coste et al., 2010). Remarkably, we did not observe any differences in Piezo1 currents upon overexpression of Mtmr2 (Figure 1-figure supplement 2b and Supplementary File 1). These results suggest a certain degree of specificity of the functional Piezo2-Mtmr2 interaction.

Next, we aimed at assessing whether Mtmr2 can modulate native Piezo2 RA-MA currents in cultured DRG neurons, as well. DRG cultures allow for the targeted manipulation of protein levels by nucleofection and concomitant assessment of Piezo2-mediated RA-MA currents (Coste et al., 2010;

Narayanan et al., 2016). It is also noteworthy, that the DRG culture system has been employed for the original discovery (Coste et al., 2010) and further characterization of Piezo2 RA-MA currents (Dubin et al., 2012; Eijkelkamp et al., 2013; Jia et al., 2016; Narayanan et al., 2016; Poole et al., 2014; Qi et al., 2015); hence it serves as a model for sensory transduction processes (Coste et al., 2007; Coste et al., 2010; Lechner and Lewin, 2009).

In order to test whether the effect on Piezo2 RA-MA currents observed in HEK293 cells can be recapitulated, we overexpressed Mtmr2 in DRG cultures and measured RA-MA currents. Similar to HEK293 cells, Mtmr2 overexpression suppressed native RA-MA currents in DRG cultures when compared to mock transfection (Figure 1g, h). The displacement threshold was unaffected upon Mtmr2 overexpression (Supplementary File 1), which is in contrast to our results in HEK293 cells potentially reflecting differences in Piezo2/Mtmr2 stoichiometry or the contribution of unknown neuronal modulators. Also, the inactivation time constant of RA-MA currents was unchanged upon overexpression of Mtmr2 in DRG neurons (Supplementary File 1).

Mtmr2 knockdown potentiates Piezo2 activity in peripheral sensory neurons

We went on to investigate whether Mtmr2 downregulation could potentiate native RA-MA currents in DRG. Successful knockdown of *Mtmr2* was achieved after 72 hours and evaluated by quantitative PCR (Figure 2-figure supplement 1a). We assessed *Piezo2* mRNA levels, Piezo2 membrane expression and the percentage of Piezo2-positive neurons and did not observe any changes upon Mtmr2 knockdown (Figure 2-figure supplement 1b-d). However, when we measured RA-MA currents in *Mtmr2* siRNA-nucleofected DRG cultures, we observed a significant augmentation in current amplitude whereas the displacement threshold and inactivation time constant were unchanged (Figure 2a-b; Supplementary File 1). These results are in agreement with our data on Mtmr2 overexpression (Figure 1) and suggest that Mtmr2 levels can modulate Piezo2 function: decreased expression of Mtmr2 potentiated, while increased expression suppressed Piezo2 RA-MA currents.

Besides Piezo2-mediated RA-MA currents, cultured DRG neurons display two other major types of MA currents: intermediately- (IA) and slowly-adapting- (SA) MA currents categorized based on their inactivation time constant (please see Methods for details) (Coste et al., 2007; Coste et al., 2010; Hu and Lewin, 2006; Lechner and Lewin, 2009). These seemed to be largely unaltered by Mtmr2 knockdown (Figure 2c, d; Supplementary File 1) indicating that mechanotransduction is not generally compromised. Remarkably though, upon Mtmr2 knockdown we detected a significant redistribution of the number of cells exhibiting MA subpopulations: a moderate increase in the proportion of RA-MA cells paralleled by a decrease of the IA-MA population (Figure 2e). To date the interpretation of the latter is difficult and requires yet to be obtained insights into the molecular nature of IA-MA currents.

Mtmr2 modulates Piezo2-mediated mechanotransduction largely via PI(3,5)P_2

Next we asked how, on a mechanistic level, Mtmr2 could regulate Piezo2 activity given that neither Piezo2 mRNA levels nor membrane expression seemed to be affected (Figure 2-figure supplement 1b,c). Mtmr2 is a phosphatase that catalyzes the removal of the 3-phosphate group from PI(3)P as well as PI(3,5)P_2 (Berger et al., 2002). Under resting conditions PI(3,5)P_2 is present at low levels (Jin et al., 2016; McCartney et al., 2014a) but is transiently and steeply generated upon a diverse range of cellular stressors. This is in contrast to intensely studied and highly abundant PI(4,5)P_2 known to

regulate ion channels (Gamper and Shapiro, 2007) including both, Piezo1 and Piezo2 (Borbiro et al., 2015).

To explore a potential role of Mtmr2 phosphatase activity and the resulting change in PIP levels (Laporte et al., 1998; McCartney et al., 2014b; Mironova et al., 2016; Previtali et al., 2007) for the regulation of Piezo2 currents, we generated a catalytically inactive Mtmr2 mutant (Mtmr2C417S) by substituting Cysteine 417 for Serine (Berger et al., 2002). If the catalysis of PIPs was essential to the functional interaction of Piezo2-Mtmr2, the catalytically inactive mutant should fail to suppress Piezo2 currents when overexpressed in HEK293 cells (please see our data on wild type Mtmr2 in Figure 1e,f). This was indeed found to be the case. Mtmr2C417S co-expression did not suppress Piezo2-mediated currents in HEK293 cells as determined by comparison of stimulus-current curves (Figure 3a) with mock transfected cells. Instead, we observed a trend towards moderate potentiation of Piezo2 currents upon co-expression of Mtmr2C417S (especially at low stimulus magnitudes; Figure 3a). This result strongly suggests that the catalytic activity of Mtmr2 and the consequential alteration of PIP levels (Laporte et al., 1998; McCartney et al., 2014b; Mironova et al., 2016; Previtali et al., 2007) may underlie the regulation of Piezo2 by Mtmr2. Importantly, enzymatically inactive Mtmr2C417S was abundantly expressed and remained capable of associating with Piezo2 in close proximity as suggested by PLA upon co-overexpression of Piezo2 and Mtmr2C417S in comparison to wild type Mtmr2 (Figure 3b-c).

Based on the results obtained from experiments with Mtmr2C417S we then proceeded to manipulate neuronal PIP levels. Figure 4a illustrates a schematic view of the PIP synthesis and turnover pathway Mtmr2 is involved in and also indicates pharmacological inhibitors known to intervene with this pathway (Vaccari et al., 2011). According to this scheme and a wealth of previous work (Laporte et al., 1998; McCartney et al., 2014b; Mironova et al., 2016; Previtali et al., 2007; Vaccari et al., 2011), knockdown of Mtmr2 would increase the levels of PI(3)P and even more $PI(3,5)P_2$ (Vaccari et al., 2011). We tried to experimentally mimic heightened levels of these PIPs by inclusion of exogenous PIPs in the intracellular recording solution (Dong et al., 2010); however, we did not see any change in RA-MA currents (Figure 4-figure supplement 1a). Due to technical factors that may confound this data (e.g. rapid breakdown of exogenous PIPs by intracellular phosphatases), we opted to perform additional experiments. We reversed the described accumulation of these two PIPs upon Mtmr2 knockdown (Laporte et al., 1998; McCartney et al., 2014b; Mironova et al., 2016; Previtali et al., 2007; Vaccari et al., 2011) by applying commonly-used inhibitors of PIP synthesis, i.e. Wortmannin, an inhibitor of the class III PI 3-kinase, (Messenger et al., 2015), and Apilimod, an inhibitor of PIKfyve (Cai et al., 2013; Vaccari et al., 2011), respectively (please see scheme in Figure 4a). If elevated levels of PI(3)P or $PI(3,5)P_2$ were implicated in Mtmr2-knockdown-induced potentiation of Piezo2, the presence of the corresponding inhibitor in the recording solution would be expected to counteract this potentiation. Wortmannin application only marginally altered the increase in RA-MA currents upon Mtmr2 knockdown in neurons (Figure 4b). Apilimod, on the other hand, significantly diminished the magnitude of RA-MA currents in *Mtmr2* siRNA-treated neurons (Figure 4b). In line with a reversal of Mtmr2-induced potentiation, the displacement threshold of RA-MA currents was significantly increased upon Apilimod treatment (Supplementary File 1). Interestingly, Apilimod treatment in wild type DRG neurons did not affect RA-MA currents (Figure 4-figure supplement 1b; Supplementary File 1), as expected given the low cellular expression and tight regulation of $PI(3,5)P_2$ under physiological conditions (Jin et al., 2016; McCartney et al., 2014a). Taken together, our results point towards a role of $PI(3,5)P_2$ for the functional interaction of Piezo2 and Mtmr2.

We then intended to assess the significance of $PI(3,5)P_2$ availability for Piezo2 function in a more physiological setting. In peripheral sensory neurons changes in cellular osmolarity cause activation of diverse ion channels and receptors followed by initiation of various signaling pathways involved in volume regulation (Lechner et al., 2011; Liu et al., 2007; Quallo et al., 2015). Interestingly, previous work has indicated that also Mtmr2, $PI(3,5)P_2$ (Berger et al., 2003; Dove et al., 1997) and Piezo2 (Jia et al., 2016) can be modulated by osmotic stress. Upon hypoosmotic stress Mtmr2 trafficking was altered and $PI(3,5)P_2$ levels were reported to be elevated in eukaryotic cells (Berger et al., 2003; Dove et al., 1997). In the case of Piezo2, hypoosmotic stress was shown to potentiate Piezo2 RA-MA currents, which was independent of the prominent osmosensor TRPV4 (Jia et al., 2016). Therefore, we employed osmotic stress as a physiological stimulus to investigate the link between Mtmr2, $PI(3,5)P_2$ and Piezo2. First, we confirmed the previously described (Jia et al., 2016) potentiation of Piezo2 RA-MA currents by application of extracellular hypotonic stress to DRG cultures (Figure 4-figure supplement 1c). We then postulated that an increase of $PI(3,5)P_2$ levels by extracellular hypotonicity (Berger et al., 2003; Dove et al., 1997) should counteract the RA-MA suppression upon Mtmr2-overexpression, which we described in Figure 1h above. Indeed, in Mtmr2 overexpressing DRG cultures we recorded significantly higher RA-MA currents under extracellular hypotonic conditions compared to isotonic conditions (Figure 4c). Other RA-MA current parameters were unchanged (Supplementary File 1). We then tested whether the opposite was also true: Would an expected decrease of $PI(3,5)P_2$ levels by intracellular hypotonicity (Dove et al., 1997) prevent RA-MA current sensitization upon Mtmr2 knockdown? Conceptually, this experiment is analogous to Apilimod application in Figure 4b above, where we pharmacologically inhibited $PI(3,5)P_2$ production in DRG cultures. As predicted, under intracellular hypotonic conditions RA-MA currents were significantly smaller in siRNA-treated cultures compared to isotonic conditions (Figure 4d; Supplementary File 1). In parallel, the displacement threshold was significantly increased, while other RA-MA current parameters remained unchanged (Supplementary File 1). As specific probes to assess the cellular distribution of $PI(3,5)P_2$ are not available (Hammond et al., 2015; Li et al., 2013b; McCartney et al., 2014a; Nicot and Laporte, 2008; Previtali et al., 2007), we could not measure the actual levels of $PI(3,5)P_2$ in neurons under different osmotic conditions. Even though, our pharmacological and osmotic experiments both suggest an interdependent contribution of Mtmr2 and $PI(3,5)P_2$ to the modulation of Piezo2-mediated MA currents in DRG cultures.

PIPs are essential membrane components and alterations of PIP availability could modify mechanical properties of cells and their membranes (Janmey, 1995; Raucher et al., 2000; Skwarekmaruszewska et al., 2006). In fact, several recent studies demonstrated the influence of membrane mechanics on mechanotransduction (Brohawn et al., 2014a; Brohawn et al., 2014b; Cox et al., 2016; Lewis and Grandl, 2015; Sukharev, 2002; Wu et al., 2016a), particularly on Piezo2-mediated RA-MA currents (Jia et al., 2016; Qi et al., 2015). Therefore, we set out to test a possible impact of Mtmr2 knockdown upon mechanical properties of cultured DRG neurons by atomic force microscopy (AFM) (Nawaz et al., 2015; Qi et al., 2015; Rehfeldt et al., 2007). However, our experiments did not show any significant differences between *Mtmr2* siRNA-treated and control-treated DRG neurons. Neither the Young´s elasticity modulus (an indicator for cellular elasticity including membrane tension and cortex stiffness) (Morley et al., 2016; Qi et al., 2015) as determined from the indentation, nor the tether force (an indicator for membrane tension and mechanical coupling to the cortex) (Qi et al., 2015) obtained from the retraction portion of the force distance curves were altered (Figure 4-figure supplement 2). These results are in line with our aforementioned findings indicating that Mtmr2 knockdown does not fundamentally alter mechanotransduction in DRG cultures (Figure 2c, d and

Supplementary File 1). Nevertheless, our AFM measurements cannot exclude possible small and local changes in membrane tension in the direct vicinity of Piezo2.

Piezo2 harbors a PIP_2 binding motif

Based on the functional role of $PI(3,5)P_2$ for Mtmr2-dependent Piezo2 regulation we investigated whether Piezo2 can bind $PI(3,5)P_2$. PIPs are known to bind to proteins through various domains such as the FYVE domain, WD40 domain, PHD domain or electrostatically via poly-basic regions with unstructured clusters of positively charged amino acid residues (Lysine or Arginine) (Dong et al., 2010; McCartney et al., 2014a). Sequence analysis revealed a region in Piezo2 with considerable similarity to the proposed $PI(3,5)P_2$ binding motif of the mucolipin TRP channel 1 (TRPML1) (Dong et al., 2010) (Figure 5a). We performed a peptide-lipid binding assay to test if this sequence in Piezo2 could bind to $PI(3,5)P_2$, which was indeed the case (Figure 5b,d). In addition, we also observed that the Piezo2 peptide was able to bind $PI(4,5)P_2$ and weakly to $PI(3,4)P_2$ (Figure 5b,d and Figure 5-figure supplement 1). This is an intriguing result because Borbiro and colleagues showed that TRPV1 modulates Piezo2 currents through $PI(4,5)P_2$ depletion, though the study did not report a $PI(4,5)P_2$ binding region in the Piezo2 sequence (Borbiro et al., 2015). In parallel we performed the binding assay with a mutated version of the Piezo2 peptide, in which positively-charged amino acid residues shown to be relevant for $PI(3,5)P_2$ binding in TRPML1 were changed to neutral Glutamine (Q; Piezo2 3Q mutant; QQILQYFWMS). This mutated peptide did not bind to any lipid (Figure 5b,d). The here identified $PI(3,5)P_2$-binding region in Piezo2 exhibits 50% sequence identity to Piezo1 with conservation of positively charged amino acid residues (Figure 5a). Therefore, we also tested whether Piezo1 was able to bind $PI(3,5)P_2$, but did not find any evidence for this (Figure 5c,d). These data suggest that not only positively charged amino acid residues, but also flanking amino acids in this Piezo2 region contribute to PIP_2 binding in a yet to be explored manner. Further, these in vitro binding studies substantiate our functional data on the specific link between Piezo2 and the Mtmr2 substrate $PI(3,5)P_2$ by identifying a $PI(3,5)P_2$ binding domain in Piezo2, but not in Piezo1. It is important to note that the peptide region defined here may not be the only $PI(3,5)P_2$ binding region in Piezo2 especially when considering the known diversity of PIP modules (Dong et al., 2010; McCartney et al., 2014a). Due to the sheer size of Piezo2 a large-scale peptide-lipid binding screen was beyond the scope of this study.

Next, we attempted to monitor the functional relevance of the here described $PI(3,5)P_2$ binding domain for the Piezo2-Mtmr2 interaction. To this end we generated a Piezo2 P1 mutant by swapping the $PI(3,5)P_2$ binding domain of Piezo2 with the corresponding domain of Piezo1 (please see scheme in Figure 5a). Remarkably, MA currents of the Piezo2 P1 mutant were only slightly attenuated upon co-expression with Mtmr2 compared to mock-transfected controls (Figure 5e). Also, the displacement threshold and inactivation time constant of MA currents remained unchanged (Supplementary File 1). This is in stark contrast to the pronounced Mtmr2-induced suppression of MA currents recorded from wildtype Piezo2 (Figure 1f). Hence, our results suggest that the $PI(3,5)P_2$ binding domain of Piezo2 identified here likely mediates the functional sensitivity of Piezo2 to Mtmr2-dependent changes in $PI(3,5)P_2$ levels.

Discussion

Vertebrate somatosensory mechanotransduction entails a complex interplay of cellular components; however, their identity is far from being resolved. In our study, we demonstrate that Mtmr2 limits

Piezo2 MA currents, and that this effect likely involves local catalysis of $PI(3,5)P_2$. Thus, our work elucidated a link between Mtmr2 and $PI(3,5)P_2$ availability as a previously unappreciated mechanism how Piezo2-mediated mechanotransduction can be locally controlled in peripheral sensory neurons.

Originally, we identified Mtmr2 as a significantly enriched member of the native Piezo2 interactome in DRG neurons (Narayanan et al., 2016). Mtmr2 is an active phosphatase that catalyzes the removal of 3-phosphate from its substrates PI(3)P and $PI(3,5)P_2$. Hence, its subcellular localization is crucial as it dictates access to its substrates, which are embedded in membrane lipid bilayers. Interestingly, several reports suggest that membrane association of Mtmr2 is enhanced by hypotonic stress (Berger et al., 2003) and also by interactions with other members of the Mtmr family (Kim et al., 2003; Ng et al., 2013). For example, Mtmr13 and Mtmr2 reciprocally control their abundance at the membrane of cultured cell lines (Ng et al., 2013; Robinson and Dixon, 2005) and in uncharacterized endomembrane compartments in Schwann cells (Ng et al., 2013). In addition, Mtmr2 enzymatic activity is augmented through interaction with Mtmr13 (Berger et al., 2006). In this respect it is noteworthy that our interactomics screen (Narayanan et al., 2016) identified two additional Mtmr family members: Mtmr1 and Mtmr5. Mtmr1 was shown to be similar to Mtmr2 in structure and substrate specificity (Bong et al., 2016), but is much less studied than Mtmr2. Mtmr5 is a catalytically inactive phosphatase which binds to Mtmr2, increases its enzymatic activity and controls its subcellular localization (Kim et al., 2003). The fact that Mtmr5 was previously reported as a binding partner of Mtmr2 further validates our published interactomics data (Narayanan et al., 2016), and hints towards the intriguing possibility that a multiprotein complex of different Mtmr family members might affect Piezo2 function. Future experiments should focus on assessing the role of these two Mtmr family members for mechanotransduction in peripheral sensory neurons.

Mechanistically, our in vitro data strongly suggest that enzymatic activity of Mtmr2 and consequently $PI(3,5)P_2$ availability modulates Piezo2 RA-MA currents. Several lines of evidence support this conclusion. We found that, unlike wild type Mtmr2, a catalytically inactive mutant of Mtmr2 (C417S) did not suppress Piezo2 currents in HEK293 cells. In sensory neurons expressing *Mtmr2* siRNA, we could counteract RA-MA current potentiation by inhibiting $PI(3,5)P_2$ synthesis in two ways: via Apilimod (Laporte et al., 1998; McCartney et al., 2014b; Mironova et al., 2016; Previtali et al., 2007; Vaccari et al., 2011) and via intracellular hypoosmolarity (Dove et al., 1997; McCartney et al., 2014a), respectively. In analogy, increasing $PI(3,5)P_2$ levels by extracellular hypoosmolarity (Berger et al., 2003; Dove et al., 1997) attenuated the suppression of RA-MA currents upon Mtmr2 overexpression. Here, it is important to note that Mtmr2 activity usually serves a dual function: dephosphorylation of $PI(3,5)P_2$ and of PI(3)P, albeit the latter with lower efficiency (Berger et al., 2002). Yet, our results upon application of Wortmannin suggest only a marginal contribution of PI(3)P to altering Piezo2-mediated mechanotransduction. Wortmannin is commonly used to block class III PI 3-kinase (please see scheme in Figure 4a), however, it also is reported to inhibit class I PI 3-kinase (Messenger et al., 2015). Hence its action on class III PI 3-kinase might not have been efficient enough in our experiments. Biologically, many enzymes control PI(3)P synthesis (Yan and Backer, 2007; Zolov et al., 2012) and previous work on Mtmr2 has only shown minor modifications of PI(3)P levels in Mtmr2-deficient cells (Cao et al., 2008; Vaccari et al., 2011) in line with its substrate preference (Berger et al., 2002). Moreover, our lipid-peptide binding assays demonstrated that, in a cell-free system, a distinct region in Piezo2, which is similar to the known $PI(3,5)P_2$-binding motif of TRPML1, can bind $PI(3,5)P_2$. Therefore, our data are highly indicative of a prominent involvement of the Mtmr2 substrate $PI(3,5)P_2$ in controlling somatosensory mechanosensitivity. Whether or not the expected

change of PI(5)P after PI(3,5)P_2 catalysis (please see scheme in Figure 4a) plays a role could not be investigated due to the lack of tools and knowledge about PI(5)P-specific physiology (McCartney et al., 2014a; Zolov et al., 2012).

Interestingly, the here identified PI(3,5)P_2-binding region is conserved among Piezo2 in vertebrates and exhibits 50% of sequence identity to mouse Piezo1 with conservation of basic amino acid residues. Arthropods and nematodes, which only encode one Piezo protein, exhibit lower sequence similarity in this region, 40% (D. melanogaster) and 30% (C. elegans), respectively. It would be of high interest to determine in future studies whether other members of the Piezo family also bind PI(3,5)P_2 and are potentially regulated by Mtmr2 or its homologs. Yet, in mice the here described PI(3,5)P_2-binding and inhibition via Mtmr2 seemed quite specific for Piezo2 as indicated by our peptide-lipid binding assays and functional experiments on the domain-swapped Piezo2 P1 mutant. In contrast to the majority of studies on the regulation of vertebrate mechanotransduction (Borbiro et al., 2015; Eijkelkamp et al., 2013; Morley et al., 2016; Poole et al., 2014; Qi et al., 2015), we did not observe alterations in Piezo1-mediated MA currents in HEK293 cells, and the magnitude of IA- and SA-MA currents was largely unaffected in DRG cultures. Surprisingly though, we detected a mild increase in the proportion of RA-MA cells paralleled by a decrease of the IA-MA subpopulation. While there is some evidence that Piezo2 might also play a role for IA-MA currents (Lou et al., 2013), to date the molecular identity of IA-MA currents has not been resolved (Viatchenko-Karpinski and Gu, 2016). For that reason the interpretation of this finding awaits further clarification of the molecular nature of IA-MA currents.

In principle, the regulation of Piezo2 by lipids is not unexpected and our data significantly advance our knowledge about the link between mechanotransduction and components of the lipid bilayer (Brohawn et al., 2014a; Brohawn et al., 2014b; Cox et al., 2016; Lewis and Grandl, 2015; Sukharev, 2002; Wu et al., 2016a). In particular, PI(4,5)P_2 and its precursor PI(4)P (Borbiro et al., 2015) as well as cholesterol (Qi et al., 2015) were recently found to be implicated in mechanotransduction mediated by both, Piezo1 and Piezo2. In contrast to PI(4,5)P_2, our understanding of PI(3,5)P_2 function, localization and regulation is limited to date (McCartney et al., 2014a). PI(3,5)P_2 is much less abundant than most PIPs, e.g. 125-fold less than PI(4,5)P_2 in mammalian cells (Zolov et al., 2012), and tightly regulated by a large protein complex (Vaccari et al., 2011; Zolov et al., 2012) (please see scheme in Figure 4a). PI(3,5)P_2 was believed to predominantly act in the endo-lysosome system of eukaryotes (Di Paolo and De Camilli, 2006; Dong et al., 2010; Ho et al., 2012; Zolov et al., 2012). By now the picture is emerging that PI(3,5)P_2 can serve a diverse range of cellular functions, such as autophagy, signaling in response to stress, control of membrane traffic to the plasma membrane as well as regulation of receptors and ion channels (Dong et al., 2010; Ho et al., 2012; Ikonomov et al., 2007; Klaus et al., 2009; McCartney et al., 2014b; Tsuruta et al., 2009; Zhang et al., 2012). Moreover, depending on the cell type, PI(3,5)P_2 synthesis and metabolism are dynamically regulated and subject to cellular stimulation and stressors, e.g. insulin-mediated PI(3,5)P_2 changes in adipocytes (Ikonomov et al., 2007), neuronal activity-dependent synthesis at hippocampal synapses (McCartney et al., 2014b; Zhang et al., 2012) and the here exploited regulation of PI(3,5)P_2 upon osmotic shock in mammalian cell lines (Dove et al., 1997; Nicot and Laporte, 2008; Previtali et al., 2007).
These reports nourish the notion that changes of PI(3,5)P_2 via Mtmr2 might contribute to regulating Piezo2 and, by extension, touch sensitivity. How could this be achieved mechanistically? Instead of acting in a cell-wide manner, PI(3,5)P_2 synthesis and turnover is confined to membrane microdomains. Despite their unknown composition and subcellular localization, these microdomains

are believed to ensure dynamic and local control of $PI(3,5)P_2$ levels (Ho et al., 2012; Jin et al., 2016; McCartney et al., 2014a). Concomitantly, the abundance of downstream effector proteins is likely to be altered, as well (Ho et al., 2012; Jin et al., 2016; McCartney et al., 2014a). Mtmr2 may physically bind to Piezo2 in order to ensure its enrichment in $PI(3,5)P_2$ microdomains, so that local $PI(3,5)P_2$ changes or yet to be identified effector proteins can efficiently modulate Piezo2 (Figure 6, working model). In these microdomains Mtmr2 would catalytically decrease $PI(3,5)P_2$ levels, which in turn could inhibit Piezo2 function. Hence, a physical interaction between Mtmr2 and Piezo2 would selectively concentrate Piezo2 at the sites of $PI(3,5)P_2$ depletion thereby allowing its inhibition in a defined membrane compartment. On the contrary, reduced Mtmr2 expression or activity would be expected to increase local $PI(3,5)P_2$ levels (Laporte et al., 1998; McCartney et al., 2014b; Mironova et al., 2016; Previtali et al., 2007; Vaccari et al., 2011) and facilitate Piezo2 potentiation. It is conceivable that Mtmr2-controlled $PI(3,5)P_2$ availability could in turn cause local changes in membrane tension (Lewis and Grandl, 2015; Perozo et al., 2002; Vásquez et al., 2014; Wu et al., 2016b). The latter has already been demonstrated to affect Piezo1 MA currents (Cox et al., 2016; Lewis and Grandl, 2015; Wu et al., 2016a). Whether Piezo2 is also sensitive to local membrane tension and whether $PI(3,5)P_2$ levels indeed influence membrane tension in sensory neurons remains to be investigated. Unfortunately, local changes in membrane tension in the vicinity of Piezo2 are likely too small to be captured by our AFM-based measurements.

Nevertheless, the data presented here allow us to infer an attractive mechanism exquisitely suited for transient and compartmentalized control of Piezo2 function, i.e. physical vicinity to Mtmr2, the activity status of Mtmr2 and consequently $PI(3,5)P_2$ availability (Figure 6). We can further speculate that this local control of Piezo2 function may serve to tune the threshold and magnitude of neuronal activity to light touch. Ultimately, Mtmr2 and $PI(3,5)P_2$ may represent a means by which touch sensitivity of an organism can be dynamically adjusted in response to diverse stimuli modulating Mtmr2 and $PI(3,5)P_2$ levels (Figure 6). In this respect it is noteworthy that multiple Mtmr2 mutations – including those affecting its activity (Berger et al., 2002) – have been implicated in Charcot-Marie-Tooth type 4B1 (CMT4B1) disease, a peripheral neuropathy characterized by abnormalities in myelination and nerve conduction (Bolino et al., 2004; Bolis et al., 2005; Bonneick et al., 2005). An analysis of Piezo2 mechanotransduction, light touch as well as tactile hypersensitivity in Mtmr2 knockout (Bolino et al., 2004) and Mtmr2 mutant mice (Bonneick et al., 2005) would be warranted to thoroughly examine the potential role of Mtmr2 for (patho)physiological aspects of vertebrate mechanosensation.

Several important questions remain to be investigated. While we identified a $PI(3,5)P_2$ binding motif in Piezo2 in vitro, we can neither gauge the affinity of the fully assembled Piezo2 trimer for $PI(3,5)P_2$ nor assess whether $PI(3,5)P_2$ and Mtmr2 bind allosterically, competitively or independently of each other. Moreover, our peptide-lipid binding assay shows that the extremely abundant $PI(4,5)P_2$ and to a lesser extent $PI(3,4)P_2$ could bind the same motif as $PI(3,5)P_2$. This raises the question how PIP_2 specificity can be achieved by Piezo2 when embedded in cellular membranes. Piezo2 might be differentially localized in membranes dependent on $PI(3,5)P_2$ levels and Mtmr2 abundance. We did not observe any differences in the overall abundance of Piezo2 channels at the plasma membrane of sensory neurons. Yet, given that $PI(3,5)P_2$ acts in membrane microdomains, it would be desirable to visualize whether Piezo2 is localized in subcellular membrane compartments, i.e. (i) in $PI(3,5)P_2$-enriched versus $PI(3,5)P_2$-depleted and/or (ii) Mtmr2-harboring versus Mtmr2-negative microdomains. It remains to be seen whether these membrane compartments are confined to the plasma membrane and/or to intracellular membranes such as endo-lysosomes, which are known to

contain the majority of PI(3,5)P_2 (Di Paolo and De Camilli, 2006; Dong et al., 2010; Zolov et al., 2012). Along these lines it is worth mentioning that AMPA receptor abundance at hippocampal synapses has been shown to be regulated by PI(3,5)P_2-controlled cycling through early and late endosomes (McCartney et al., 2014b). While unknown so far, localization of Piezo2 to intracellular membranes would not be unexpected (Coste et al., 2010) since its family member Piezo1 has originally been described to reside in the endoplasmic reticulum (McHugh et al., 2010). Thus, exploring endocytosis and intracellular trafficking of Piezo2 may offer novel insights into its regulation by the intracellular membrane pool of PI(3,5)P2.

To address some of these issues the development of high-affinity Mtmr2 and Piezo2 antibodies as well as PI(3,5)P_2-specific probes (Hammond et al., 2015; Li et al., 2013b; McCartney et al., 2014a; Nicot and Laporte, 2008; Previtali et al., 2007), which faithfully represent their subcellular spatial and temporal dynamics, would be required. In contrast to PI(4,5)P_2, such probes have not yet been successfully designed for PI(3,5)P_2, and the value of the few existing probes is questionable due to spatial restrictions and limited specificity for PI(3,5)P_2 (Hammond et al., 2015; Li et al., 2013b; McCartney et al., 2014a; Nicot and Laporte, 2008; Previtali et al., 2007). Future studies using these tools combined with high-resolution microscopy have the potential to address fundamental aspects of Piezo2 trafficking, localization, and function.

Taken together, our data present Mtmr2 as a novel modulator of the mechanosensory apparatus, and we provide evidence for the functional convergence of Mtmr2 enzymatic activity and PI(3,5)P_2 availability onto Piezo2-mediated mechanotransduction in peripheral sensory neurons. In essence, we propose the Mtmr2-Piezo2 interaction as a previously unappreciated mechanism to locally and dynamically regulate Piezo2 function and, consequently, the organism´s response to light tough. Therefore, our study significantly advances our understanding of the complex molecular machinery underlying somatosensory mechanosensitivity in vertebrates.

Methods

Key Resources Table

Reagent type (species) or resource	Designation	Source or reference	Identifiers	Additional information
strain, strain background (mouse)	B6/J mice		RRID: IMSR_JAX:000664	bred in the animal facility of the MPIem Goettingen
strain (mouse)	Piezo2GFP	kind gift of Ardem Patapoutian		bred in the animal facility of the MPIem Goettingen
cell line (human)	HEK293	purchased from ATCC	RRID: CVCL_0045	Cells were not tested for mycoplasma contamination; cells were authenticated by ATCC upon purchase
antibody	Rabbit anti-Mtmr2 (1:100)	Biotechne, #NBP1-33724	RRID: AB_2147841	
	Chicken anti-GFP (1:500)	Life, #A10262	RRID: AB_2534023	
	Rabbit anti-GST (1:500)	Santa Cruz, #sc-459		
	Mouse anti-	Santa Cruz,	RRID: AB_627266	

	myc (1:750, 1:500)	#sc-47694		
	Mouse anti-FLAG (1:100)	Sigma Aldrich, #F1804	RRID: AB_262044	
	Rabbit anti-Piezo2 (1:200)	Novus Biologicals, #NBP1-78624	RRID: AB_11005294	
recombinant DNA reagent	pCMVSport6 Piezo2-GST IRES GFP	kind gift of Ardem Patapoutian	mouse *Piezo2*	
	pCMV6-Entry Mtmr2-myc-DDK	Origene, #MR215223	mouse *Mtmr2*	
	Mtmr2C417S-myc-DDK		mouse *Mtmr2 C417S*	Mutation generated using Q5® Site-Directed Mutagenesis kit (New England BioLabs)
	pCMV Sport6 Piezo1-753-myc-IRES GFP	kind gift of Ardem Patapoutian	mouse *Piezo1*	Myc tag was inserted at amino acid 753 as described in Coste et al., Nature Communications, 2015.
	pGEM-Teasy Kv1.1-HA		Mouse *Kv1.1*	
	pCMVSport6			
	pCDNA3.1-myc-His	Invitrogen, #V80020		
	pCNDA3-GST	kind gift of Ardem Patapoutian		
	pCMVSport6 Piezo2 P1 mutant-GST IRES GFP		mouse *Piezo2 P1* mutant	Mutation generated using Q5® Site-Directed Mutagenesis kit (New England BioLabs)
	pCDNA3.1-myc-His TRPA1	kind gift of Ardem Patapoutian	mouse TRPA1	
	pCMV6-Vti1b-myc-DDK	Origene		
sequence-based reagent	*Mtmr2* forward primer for qPCR	MPIem DNA Core Facility	TGTACCCCACCATTGAAGAAA	
	Mtmr2 reverse primer for qPCR	MPIem DNA Core Facility	TAAGAGCCCCTGCAAGAATG	
	Piezo2 forward primer for qPCR	MPIem DNA Core Facility	AGGCAGCACATAGGATGGAT	
	Piezo2 reverse primer for qPCR	MPIem DNA Core Facility	GCAGGGTCGCTTCAGTGTA	
	Actb forward primer for qPCR	MPIem DNA Core Facility	GATCAAGATCATTGCTCCTCCTG	
	Actb reverse primer for qPCR	MPIem DNA Core Facility	CAGCTCAGTAACAGTCCGCC	
	Gapdh forward primer for	MPIem DNA Core Facility	CAATGAATACGGCTACAGCAAC	

	qPCR			
	Gapdh reverse primer for qPCR	MPIem DNA Core Facility	TTACTCCTTGGAGGCCATGT	
	Piezo2 mutagenesis forward primer	MPIem DNA Core Facility	GTCTTCTGGTGGCTCGTGGTCATTTATACCATGTTGG	
	Piezo2 mutagenesis reverse primer	MPIem DNA Core Facility	ACGCAGCAGCTTCCTCCACCACTCGTAGTGCAC	
	Mtmr2 mutagenesis forward primer	MPIem DNA Core Facility	GTGGTACACTCCAGTGATGGATG	
	*Mtmr2*mutagenesis reverse primer	MPIem DNA Core Facility	CACAGACGTCTTCCCAGA	
peptide, recombinant protein	Piezo2-FLAG tagged	Custom-made by GenScript	EWWRKILKYFWMSVVIDYKDDDDKQNN	
	Piezo2 3Q-FLAG tagged	Custom-made by GenScript	EWWQQILQYFWMSVVIDYKDDDDKQNN	
	Piezo1-FLAG tagged	Custom-made by GenScript	TLWRKLLRVFWWLVDYKDDDDKQNN	
chemical compound, drug	Wortmannin	Sigma Aldrich		
	Apilimod	Bertin Pharma		
	PI(3,5)P2	Echelon		
	PI(3)P	Echelon		
software, algorithm	Fitmaster	HEKA Electronik GmbH		
	Patchmaster	HEKA Electronik GmbH		
	ImageJ	NIH (Schindelin et al., 2015)	RRID: SCR_003070	
	GraphPad Prism 6.01	GraphPad Software	RRID: SCR_015807	

DRG culture and transfection

Preparation and culture of mouse DRG neurons were performed as described previously (Coste et al., 2010; Narayanan et al., 2016). Throughout the study, DRG were isolated from 9-10 week old male C57BL/6J mice or, in case of experiments in Figure 1a, Figure 1-figure supplement 1a,c, Figure 2-figure supplement 1c,d from *Piezo2*^{GFP} mice (Woo et al., 2014). In brief, DRG neurons were promptly isolated and digested with collagenase (Life Technologies) and papain (Worthington). Neurons were plated on poly-D-lysine (1mg/mL, Milipore) coated coverslips, which were additionally coated with laminin (20 µg/mL, Life Technologies). Growth medium (Hams F12/DMEM 1:1 ratio with L-glutamine; Gibco) was supplemented with 10% horse serum (Life Technologies) and 100 ng/ml NGF, 50 ng/ml GDNF, 50 ng/ml BDNF, 50 ng/ml NT-3, and 50 ng/ml NT-4 (all growth factors procured from R&D Systems).

Transfection of neurons was achieved by nucleofection of siRNA or plasmid into freshly isolated DRG neurons using the P3 Primary Cell 4D Nucleofector X Kit with the 4D-Nucleofector X Unit according to the manufacturer's instructions (Lonza AG). 500 nM FlexiTube GeneSolution *Mtmr2* siRNA (Qiagen, #GS77116) or AllStar Negative control siRNA (CTRL, Qiagen, #SI03650318) for knockdown in DRG neurons and 0.5 µg of pCMV6 *Mtmr2-myc-DDK* (Origene) or 0.5 µg of pCMVSport6 or pcDNA3.1 myc-His (CTRL) for overexpression in DRG neurons, was used. After nucleofection, neurons were allowed to recover in calcium free RPMI medium (Life Technologies) for 10 min at 37°C before plating in growth medium. Two hours after transfection half of the growth medium was exchanged with fresh medium and neurons were grown for 48-72 hours before being used for electrophysiology, immunostaining or qPCR.

HEK293 cell culture and transfection

HEK293 cells were authenticated by ATCC upon purchase. Thereafter, cell line identity was authenticated by regular morphological inspection. Symptoms for mycoplasma contamination were not observed and thus no test for mycoplasma contamination was performed. Cells were cultured in DMEM with Glutamax (Thermo Fisher Scientific) supplemented with 10% FBS (Fetal bovine serum, Life Technologies) and 5% Pen/Strep (Life Technologies). Cells were grown up to 80-90% confluence before being used for transfection. Transfection was done using Fugene HD Transfection reagent (Promega). Cells were plated on poly-D-lysine-coated coverslips and maintained in culture for 48 hours before being used for electrophysiology or proximity ligation assay (PLA).

cDNA and plasmids

pCMVSport6 *Piezo2-GST*-IRES GFP (kind gift from Prof. Ardem Patapoutian, La Jolla); pCMV6-Entry *Mtmr2-myc-DDK* (Origene, #MR215223); pCMV6-Entry *Mtmr2C417S-myc-DDK* (mutation as described in (Berger et al., 2002); pCMV Sport6 *Piezo1-753-myc*-IRES GFP (kind gift from Ardem Patapoutian, La Jolla) (Coste et al., 2015); pGEM-Teasy *Kv1.1-HA*; pCMVSport6; pCDNA3.1-myc-His (Invitrogen, #V80020); pCNDA3-GST (kind gift from Prof. Ardem Patapoutian, La Jolla); pCMVSport6 *Piezo2 P1 mutant-GST*-IRES GFP. *Mtmr2C417S* mutant and *Piezo2 P1* mutant were prepared using Q5® Site-Directed Mutagenesis kit (New England BioLabs). Mutagenesis was done according to manufactures instructions and all mutant plasmids were verified by sequencing. Primers used for the mutagenesis were as follows: *Mtmr2* mutagenesis forward primer: GTGGTACACTCCAGTGATGGATG; *Mtmr2* mutagenesis reverse primer: CACAGACGTCTTCCCAGA; *Piezo2* mutagenesis forward primer: GTCTTCTGGTGGCTCGTGGTCATTTATACCATGTTGG; *Piezo2* mutagenesis reverse primer: ACGCAGCAGCTTCCTCCACCACTCGTAGTGCAC.

Quantitative PCR (qPCR)

Total RNA was isolated from cultured DRG neurons (transfected with *Mtmr2* siRNA or CTRL, please see above), using NucleoSpin RNA XS (Macherey-Nagel) according to the manufacturer's instructions. First-strand cDNA synthesis was done using QuantiTect reverse transcription kit (Qiagen). Mtmr2 and Piezo2 gene expression was assessed in both conditions by real-time qPCR using the SYBR green system (Power SYBR Green PCR Master Mix; Life Technologies) on a LightCycler 480 instrument (Roche). The melting curve analysis of amplified products was used to confirm the specificity of qPCR assay. All samples were run in triplicate and negative control reactions were run without template. Threshold cycle (Ct) values, the cycle number in which SYBR green fluorescence rises above

background, were normalized to two reference genes (*Actb* and *Gapdh*) and recorded as a measure of initial transcript amount. Relative quantification was performed using the 'fit point' as well as the 'second derivative maximum' method of the LightCycler 480. Primer sequences 5'-3' are the following: *Mtmr2* (fw: TGTACCCCACCATTGAAGAAA; rev: TAAGAGCCCCTGCAAGAATG), *Piezo2* (fw: AGGCAGCACATAGGATGGAT; rev: GCAGGGTCGCTTCAGTGTA), *Actb* (fw: GATCAAGATCATTGCTCCTCCTG; rev: CAGCTCAGTAACAGTCCGCC), *Gapdh* (fw: CAATGAATACGGCTACAGCAAC; rev: TTACTCCTTGGAGGCCATGT). Of note, only data normalized to *Actb* are shown but data normalized to *Gapdh* gave similar results. Our qPCR results indicate successful siRNA-mediated knockdown of Mtmr2 across the whole coverslip, which also includes non-transfected neurons and glia cells. Therefore our data do not report on the transfection efficiency and extent of Mtmr2 knockdown in individual neurons.

Electrophysiology

Whole-cell voltage clamp recordings were performed in transfected DRG cultures, wild type DRG cultures or transfected HEK293 cell cultures at room temperature as described in (Narayanan et al., 2016). Briefly, (protocol adapted from (Coste et al., 2010)) to elicit mechanically activated currents, the cell soma was mechanically stimulated using a blunt probe (fire polished borosilicate glass capillary). The stimulation was delivered using a piezo-electrically driven micromanipulator (Physik Instrumente GmbH&Co.KG). The probe was initially positioned ~4 µm from the cell body and had a velocity of 0.8 µm/ms during the ramp phase (forward motion). The stimulus was applied for 150 ms with an inter-stimulus interval of 180 ms. Stimulus-current measurements were performed using mechanical stimulations from 0 to 6 µm in 1 µm increments at a holding potential of -70 mV in whole cell mode. All recordings other than specifically indicated were made in standard extracellular solution containing (in mM) 127 NaCl, 3 KCl, 1 $MgCl_2$, 2.5 $CaCl_2$, 10 Glucose and 10 HEPES; pH = 7.3; osmolarity = 285 mOsm (Coste et al., 2010). To achieve hypotonicity the extracellular solution was adjusted to 160 mOsm. The intracellular solution for DRG neurons contained (in mM) 133 CsCl, 10 HEPES, 5 EGTA, 1 $MgCl_2$, 1 $CaCl_2$, 4 MgATP and 0.4 NaGTP; pH = 7.3; osmolarity = 280 mOsm (Coste et al., 2010). Hypotonic intracellular solution contained (in mM) 65 CsCl, 10 HEPES, 5 EGTA, 1 $MgCl_2$, 1 $CaCl_2$, 4 MgATP and 0.4 NaGTP; pH=7.3; osmolarity = 162 mOsm. Intracellular solution for HEK293 cells contained (in mM) 110 KCl, 10 NaCl, 1 $MgCl_2$, 1 EGTA and 10 HEPES; pH = 7.3 (Poole et al., 2014). Based on protocols published elsewhere (Jia et al., 2016) recordings in extracellular hypotonic solutions were performed as follows: Cells were incubated with the hypotonic solution for 5 minutes at 37°C prior to recording, after which RA-MA currents were recorded in hypotonic extracellular solution between 0-20 minutes after initial application. For some experiments described in this study, DRG neurons were treated with chemical inhibitors of the phosphatidylinositol phosphate pathway. Cells were treated with 35 µM Wortmannin (Sigma Aldrich; protocol adapted from (Mo et al., 2009)) in DMSO or 1 µM Apilimod (Bertin Pharma; protocol adapted from (Mironova et al., 2016)) in DMSO for 2 hours prior to recording. DMSO (0.08% for Apilimod and 0.35% for Wortmannin), was used as vehicle for each experiment. For PIP addition experiments, 1 µM $PI(3,5)P_2$ (Echelon) or 1 µM PI(3)P (Echelon) were included in the isotonic intracellular solution (protocol adapted from (Dong et al., 2010)). Of note, the water-soluble diC8 form of the lipids was used as indicated elsewhere (Dong et al., 2010).

Data analysis and representation was done using Fitmaster (HEKA Electonik GmbH, Germany) and Igor Pro 6.37 (WaveMetrics, USA). The current magnitude was calculated by measuring peak amplitudes (at each stimulus point) and subtracting leak current.

The displacement threshold was defined as the minimum displacement required to elicit a visible RA-MA current, i.e. the displacement at which current values exceeded 100 pA in DRG (Jia et al., 2016; Narayanan et al., 2016) and 50pA in HEK293 cells (Szczot et al., 2017). In HEK293 cells, this cutoff also served to prevent contamination of recordings by HEK293 endogenous Piezo1 (Dubin et al., 2017; Szczot et al., 2017). Of note, responses in HEK293 cells increased proportionally to stimulus strength and were absent in cells not transfected with *Piezo1* or *Piezo2* plasmids.

For measurements of inactivation kinetics current traces reaching at least 75% of maximal current amplitude were fitted with a mono-exponential or bi-exponential equation and the fast time constant was used for analysis (Coste et al., 2010). Data for the displacement threshold and inactivation time constant (τ) are provided in Supplemental table 1.

In DRG cultures neuronal soma size differs considerably within a coverslip. Therefore neurons have been traditionally categorized into small, medium and large diameter neurons (Drew et al., 2004; Hu and Lewin, 2006; Patapoutian et al., 2009; Woo et al., 2014)exhibiting well-reported differences in function and MA currents (Drew et al., 2004; Hu and Lewin, 2006; Patapoutian et al., 2009; Poole et al., 2014; Woo et al., 2014). To account for variability of our data due to soma size, we (i) recorded RA currents from visibly large diameter neurons (cell capacitance > 40 pF) likely representing mechanoreceptors (Drew et al., 2004; Hu and Lewin, 2006; Poole et al., 2014; Woo et al., 2014), (ii) analyzed SA currents from small diameter neurons (cell capacitance < 30 pF) likely representing nociceptors (Drew et al., 2004; Hu and Lewin, 2006; Poole et al., 2014; Woo et al., 2014) and (iii) additionally normalized all obtained current data to the individual cell capacitance to obtain a value for current density (pA/pF). The latter analysis (data not shown) yielded similar results as the presented analysis based on current amplitudes for all DRG datasets in this manuscript. IA currents were randomly recorded across all neuron sizes.

Of note, current amplitudes and displacement thresholds cannot be compared among experimental datasets because of differential treatments (e.g. nucleofection, inhibitors) requiring measurements at different culture days in vitro (DIV), and due to the inherent variability in DRG cultures dependent on mouse cohorts used throughout the course of this study. For this reason each dataset consists of experiments and respective controls measured in parallel (i) in the same mouse cohort and (ii), where possible, on each experimental day. For each dataset (experimental versus control conditions) several coverslips from at least 4 (range: 4-18) independent cell cultures or 2-12 independent platings of HEK293 cells were used.

Immunostaining and analysis

Immunostaining was carried out as described (Narayanan et al., 2016). Briefly, *Piezo2*^{GFP} mice (Woo et al., 2014) (ages 8-9 weeks) were euthanized with CO_2 or perfused with 4% PFA (Science Services). DRG neurons were isolated and cultured using the protocol described above or DRG were carefully dissected, collected in 4% PFA/1X PBS, and post-fixed for 30 minutes at 4°C. After overnight cryoprotection in 30% sucrose tissues were frozen in optimal cutting temperature medium, sectioned with a cryostat into 10 µm thick sections, mounted on SuperFrost Plus slides, and stored at −80°C. Frozen slides were thawed at room temperature for 30 min, washed thrice with 1X PBS, blocked for 30 min in 1X PBS containing 5% goat or donkey serum (Dianova) and 0.4% TritonX-100 (Roth), and incubated with primary antibodies (diluted in 0.1% TritonX-100 and 1% serum in 1X PBS), overnight at 4°C. The sections were then washed with 1X PBS and incubated for 2 hours at room temperature with secondary antibodies diluted 1:250 in 0.1% TritonX-100 and 1% serum in 1X PBS. Sections were

then washed six times with 1X PBS and mounted in SlowFade Gold antifade reagent with DAPI (Life Technologies).

For cultured DRG neurons, coverslips containing cells were washed with 1X PBS and fixed in 4% PFA for 10 minutes. Thereafter cells were washed with 1X PBS and blocked with blocking solution containing 5% serum and 0.4% TritonX-100. Cells were then incubated with primary antibodies (diluted in 1% serum and 0.1% TritonX-100), overnight at 4°C. Cells were then washed with 1X PBS and incubated with secondary antibodies (diluted in 1% serum and 0.1% TritonX-100) for 2 hours at room temperature followed by additional washes. Coverslips were mounted onto SuperFrost Plus slides using SlowFade Gold reagent with DAPI (Life Technologies).

WGA staining to mark membranes of cells was done as follows; before fixation, the cells were treated with WGA-555 (1:200) for 15 minutes at 37°C. Cells were then washed three times with medium and the standard immunostaining protocol was performed.

Imaging was done using a Zeiss Axio Observer Z1 inverted microscope or a Zeiss LSM 510 Meta Confocal microscope. All images were processed and analyzed by ImageJ, NIH (Schindelin et al., 2015).

For the analysis of Mtmr2 in cryo-frozen sections or primary cultures of DRGs from *Piezo2*^{GFP} mouse, sections were stained with anti-GFP and anti-Mtmr2 antibodies. Positive cells were identified by setting the threshold as 'mean intensity+3*standard deviation' of randomly selected (~10) negative cells. The numbers of positive and negative cells were counted using the "cell counter" plugin of ImageJ. Only for presentation purposes brightness, contrast and levels of images were adjusted in Adobe Photoshop. In all cases image adjustments were applied equally across the entire image and equally to controls.

For the analysis of membrane intensity of Piezo2-GFP upon Mtmr2 knockdown, the "analyze particle tool" from ImageJ was used. The WGA staining was used to mark the region of interest around the cell membrane and for each ROI, the mean intensity (arbitrary units, AU) and area of positive signal was determined. The mean intensity of signal (arbitrary units, AU) was calculated by subtracting the threshold (defined as 'mean+3*standard deviation' of background) from the total mean intensity.

Proximity ligation assay (PLA)

PLA was carried out as described (Hanack et al., 2015; Narayanan et al., 2016) with minor modifications. HEK293 cells or DRG neurons were plated on MatTek dishes coated with poly-D-lysine (and Laminin for DRG neuron cultures) and transfected with appropriate plasmids (details of plasmids are provided below). Cells were cultured for 48 hours before staining. Cells were washed with 1X PBS and fixed with 4% PFA for 10 minutes at room temperature. Thereafter cells were blocked in Duolink Blocking Solution (Sigma Aldrich) for 2 hours at room temperature. Cells were then incubated with primary antibodies (diluted in Duolink Antibody Diluent (Sigma Aldrich)), overnight at 4°C. Cells were washed with wash buffer A (0.01 M Tris, 0.15 M NaCl and 0.05% Tween 20, pH 7.4) and incubated with PLA probes (PLUS and MINUS probes were diluted 1:10 in Duolink antibody diluent (Sigma Aldrich)) for 1 hour at 37°C. Cells were washed again with wash buffer A and incubated with amplification mix (amplification stock 1:5 and polymerase 1:80 in water) for 100 minutes at 37°C. Cells were then washed with wash buffer B (0.2 M Tris, 0.1 M NaCl, pH7.5) and stored in 1X PBS before imaging. Secondary controls meant omitting all primary antibodies.

Plasmids used: pCMVSport6 *Piezo2-GST*-IRES-GFP (kind gift from Prof. Ardem Patapoutian); pCMV6-Entry *Mtmr2-myc-DDK* (Origene, #MR215223); pCMV6-Entry *Mtmr2C417S-mycDDK*, mutation as described by Berger and colleagues (Berger et al., 2002), was custom-generated using the Q5® Site-

Directed Mutagenesis kit (New England BioLabs); pCMVSport6; pCDNA3.1-myc-His (Invitrogen, #V80020); pmaxGFP®Vector (Lonza).

The PLA was imaged using a Zeiss Axio Observer Z1 inverted microscope. The imaging settings were constant across all samples of the same experiments. Secondary controls were always imaged in parallel using the same settings. Image analysis was done using ImageJ. The background was determined as the 'mean intensity+3*standard deviation' of randomly chosen negative cells per field of view and averaged for all images within one condition. The highest background value was then used as threshold for the analysis. GFP positive cells (from Piezo2-GST-IRES-GFP expression or pmaxGFP®Vector) were chosen for each field of view and the PLA signal was analyzed for these cells, using the "Analyze Particle" tool of ImageJ. The number of PLA puncta and total area of positive PLA signal for each cell was measured. To account for variability in cell size, the total area of the cell was also measured and the PLA signal values were normalized to total cell area. Only for presentation purposes brightness, levels and contrast of images were adjusted in Adobe Photoshop. In all cases image adjustments were applied equally across the entire image and equally to controls. Experiments were performed on several coverslips of at least two independently transfected HEK293 and DRG cultures, respectively.

Atomic force microscopy, AFM

DRG neurons were nucleofected with AllStar Negative control siRNA (CTRL) or *Mtmr2* siRNA, as described above, and maintained in culture for 72 hours. Elasticity and tether force measurements were performed with an AFM (MFP-3D extended head, Asylum Research) mounted on an inverted microscope (IX71, Olympus) using contact mode with a triangular cantilever comprising a pyramidal tip (TR-400-PB, Olympus). During the measurements cells were maintained in growth media. The spring constant of the cantilever was determined using the built in thermal method (24-28 pN/nm). Indentation and retraction speed was kept constant at 5 µm/s, and force load of 200-1000 pN was used to measure the Young's modulus of the cells. The effective Young's modulus E_{eff} was fitted with a modified Hertz model using a self-written IGOR macro (Rehfeldt et al., 2007). Tether forces were determined as the difference of pulling force before and after rupture of a tether from the AFM tip using a semi-automated step finding procedure (Nawaz et al., 2015).

Bioinformatic identification of PIP2 binding regions in Piezo2

TRPML1 is known to bind $PI(3,5)P_2$ through a region in its N-terminus (Dong et al., 2010). This region of TRPML1 (NP_444407.1) was compared to mouse Piezo2 (NP_001034574.4) and mouse Piezo1 (NP_001032375.1) using NCBI protein Blast (National Library of Medicine (US), National Center for Biotechnology Information).

Peptide-lipid binding assay

The protocol was adapted from (Berger et al., 2002) with minor modifications. In brief, PIP strips (Echelon Biosciences, Inc.) were washed once with PBS-T (1x PBS +1% Tween) and blocked with 3% fat free BSA (bovine serum albumin; Sigma Aldrich) in 1X PBS for 1 hour at room temperature. The membranes were then incubated with 0.5 µg/mL peptide solution (peptide dissolved in 1% BSA) for 2 hours at room temperature. Experiments and controls were processed in parallel. Membranes were washed with PBS-T three times for 7 minutes each and then incubated with primary antibody at room temperature for 2 hours. Membranes were then washed with PBS-T and probed with secondary antibodies coupled with Alexa680 for 1 hour at room temperature. Imaging was done on

the Odyssey Infrared System (LI-COR). Only for presentation purposes brightness, gradient levels and contrast of images were adjusted in Adobe Photoshop. In all cases image adjustments were applied equally across the entire image and equally to controls.

Peptides

The following peptides were used in this study (all procured from GenScript): Piezo2 (731-746)-FLAG tagged [EWWRKILKYFWMSVVIDYKDDDDKQNN]; Piezo2 3Q mutant (731-746)-FLAG tagged [EWWQQILQYFWMSVVIDYKDDDDKQNN]; Piezo1 (626-639)-FLAG tagged [TLWRKLLRVFWWLVDYKDDDDKQNN].

Antibodies

The following antibodies were used in this study: 1:100 rabbit anti-Mtmr2 (Biotechne, #NBP1-33724); 1:500 chicken anti-GFP (Life, #A10262); 1:250 (Immunocytochemistry), 1:500 (PLA) rabbit anti-GST (Santa Cruz, #sc-459); 1:100 (immunocytochemistry and immunoblotting), 1:750, 1:500 (PLA in HEK293 cells and DRG neurons respectively) mouse anti-myc (Santa Cruz, #sc-47694); 1:200 Rabbit anti-Piezo2 (Novus Biologicals, #NBP1-78624); 1:500 mouse anti-FLAG (Sigma Aldrich, #F1804), Secondary antibodies conjugated to Alexa Fluor 488, Alexa Fluor 546, Alexa Fluor 647, Alexa Fluor 680 (Life Technologies), Duolink in situ PLA probes 1:10 anti-rabbit MINUS, 1:10 anti-mouse PLUS.

Statistics

Data was analyzed using GraphPad Prism 6.01 (San Diego, USA). All data are represented as mean ± SEM (standard error of mean) unless indicated otherwise. All replicates were biological. All statistical tests are two-sided unless indicated otherwise. In all panels: ns>0.05; *p≤0.05; **p≤0.01; *** p≤0.001; **** p≤0.0001).

PLA data: Mann-Whitney test or Kruskal-Wallis test with Dunn's Multiple Comparison test.

Atomic force microscopy (AFM) data: Mann-Whitney test.

qPCR: One sample t-test was used (values were compared to a theoretical mean of 1.00, i.e. mRNA expression in CTRL).

Immunostaining: For membrane Piezo2 expression and number of Piezo2-positive neurons upon Mtmr2 knockdown, the Mann-Whitney test was used.

Peptide-lipid binding assays: One-way ANOVA followed by Dunnett´s or Holm-Sidak's multiple comparisons test was used as indicated.

Electrophysiology: For the analysis of stimulus-current curves, 2-way ANOVA with Holm-Sidak's multiple comparisons test was used. The P-value represents the results of 2-way ANOVA, testing the overall effect of the respective treatment. Results of the Holm-Sidak's multiple comparisons test are represented by p-values and indicated in each legend. Outlier analysis was carried out using the Grubb's test followed by testing whether the outlier value exceeded 'mean+3* standard deviation'. Outlier analysis was only performed on current values at maximal stimulation. Only if a value met both criteria (Grubb's outlier and >'mean+3*standard deviation') the cell was excluded from further analysis. Datasets, where a single outlier was removed: Figure 1h, Figure 2b, Figure 4b, Figure 4d, Figure 4-figure supplement 1a,c. For the analysis of the displacement threshold and inactivation time constant the Mann-Whitney test was used, unless more than two groups were compared, for which one-way ANOVA or Kruskal-Wallis test followed by Dunn's multiple comparisons test were used. For

the analysis of mechanically activated (MA) current populations Chi-square test was used and data are represented as % of all analyzed cells.

References

Begley, M.J., Taylor, G.S., Brock, M.A., Ghosh, P., Woods, V.L., and Dixon, J.E. (2006). Molecular basis for substrate recognition by MTMR2, a myotubularin family phosphoinositide phosphatase. Proc Natl Acad Sci U S A *103*, 927-932.

Berger, P., Berger, I., Schaffitzel, C., Tersar, K., Volkmer, B., and Suter, U. (2006). Multi-level regulation of myotubularin-related protein-2 phosphatase activity by myotubularin-related protein-13/set-binding factor-2. Human Molecular Genetics *15*, 569-579.

Berger, P., Bonneick, S., Willi, S., Wymann, M., and Suter, U. (2002). Loss of phosphatase activity in myotubularin-related protein 2 is associated with Charcot-Marie-Tooth disease type 4B1. Human molecular genetics *11*, 1569-1579.

Berger, P., Schaffitzel, C., Berger, I., Ban, N., and Suter, U. (2003). Membrane association of myotubularin-related protein 2 is mediated by a pleckstrin homology-GRAM domain and a coiled-coil dimerization module. Proceedings of the National Academy of Sciences of the United States of America *100*, 12177-12182.

Bolino, A., Bolis, A., Previtali, S.C., Dina, G., Bussini, S., Dati, G., Amadio, S., Del Carro, U., Mruk, D.D., Feltri, M.L*., et al.* (2004). Disruption of Mtmr2 CMT4B1-like neuropathy with myelin outfolding and impaired spermatogenesis. Journal of Cell Biology *167*, 711-721.

Bolino, A., Marigo, V., Ferrera, F., Loader, J., Romio, L., Leoni, A., Di Duca, M., Cinti, R., Cecchi, C., Feltri, M.L*., et al.* (2002). Molecular characterization and expression analysis of Mtmr2, mouse homologue of MTMR2, the myotubularin-related 2 gene, mutated in CMT4B. Gene *283*, 17-26.

Bolis, A., Coviello, S., Bussini, S., Dina, G., Pardini, C., Previtali, S.C., Malaguti, M., Morana, P., Del Carro, U., Feltri, M.L*., et al.* (2005). Loss of Mtmr2 phosphatase in Schwann cells but not in motor neurons causes Charcot-Marie-Tooth type 4B1 neuropathy with myelin outfoldings. J Neurosci *25*, 8567-8577.

Bong, S.M., Son, K.-B., Yang, S.-W., Park, J.-W., Cho, J.-W., Kim, K.-T., Kim, H., Kim, S.J., Kim, Y.J., and Lee, B.I. (2016). Crystal Structure of Human Myotubularin-Related Protein 1 Provides Insight into the Structural Basis of Substrate Specificity. PloS one *11*, e0152611.

Bonneick, S., Boentert, M., Berger, P., Atanasoski, S., Mantei, N., Wessig, C., Toyka, K.V., Young, P., and Suter, U. (2005). An animal model for Charcot-Marie-Tooth disease type 4B1. Human Molecular Genetics *14*, 3685-3695.

Borbiro, I., Badheka, D., and Rohacs, T. (2015). Activation of TRPV1 channels inhibits mechanosensitive Piezo channel activity by depleting membrane phosphoinositides. Science Signalling *8*, 1-12.

Brohawn, S.G., Campbell, E.B., and MacKinnon, R. (2014a). Physical mechanism for gating and mechanosensitivity of the human TRAAK K+ channel. Nature *516*.

Brohawn, S.G., Su, Z., and MacKinnon, R. (2014b). Mechanosensitivity is mediated directly by the lipid membrane in TRAAK and TREK1 K+ channels. Proceedings of the National Academy of Sciences of the United States of America *111*.

Cai, X., Xu, Y., Cheung, A.K., Tomlinson, R.C., Alcazar-Roman, A., Murphy, L., Billich, A., Zhang, B., Feng, Y., Klumpp, M*., et al.* (2013). PIKfyve, a class III PI Kinase, is the target of the small molecular IL-12/IL-23 inhibitor apilimod and a player in toll-like receptor signaling. Chemistry and Biology *20*, 912-921.

Cao, C., Backer, J.M., Laporte, J., Bedrick, E.J., and Wandinger-Ness, A. (2008). Sequential Actions of Myotubularin Lipid Phosphatases Regulate Endosomal PI(3)P and Growth Factor Receptor Traffickin. Molecular Biology of the Cell *19*, 3334-3346.

775 Coste, B., Crest, M., and Delmas, P. (2007). Pharmacological Dissection and Distribution of
776 NaN/Nav1.9, T-type Ca ²⁺ Currents, and Mechanically Activated Cation Currents in
777 Different Populations of DRG Neurons. The Journal of General Physiology *129*, 57-77.
778 Coste, B., Mathur, J., Schmidt, M., Earley, T.J., Ranade, S., Petrus, M.J., Dubin, A.E., and Patapoutian,
779 A. (2010). Piezo1 and Piezo2 are essential components of distinct mechanically-activated cation
780 channels. Science *330*, 55-60.
781 Coste, B., Murthy, S.E., Mathur, J., Schmidt, M., Mechioukhi, Y., Delmas, P., and Patapoutian, A.
782 (2015). Piezo1 ion channel pore properties are dictated by C-terminal region. Nature
783 communications *6*, 7223.
784 Coste, B., Xiao, B., Santos, J.S., Syeda, R., Grandl, J., Spencer, K.S., Kim, S.E., Schmidt, M., Mathur, J.,
785 Dubin, A.E.*, et al.* (2012). Piezo proteins are pore-forming subunits of mechanically activated
786 channels. Nature *483*, 176-181.
787 Cox, C.D., Bae, C., Ziegler, L., Hartley, S., Nikolova-Krstevski, V., Rohde, P.R., Ng, C.-A., Sachs, F.,
788 Gottlieb, P.a., and Martinac, B. (2016). Removal of the mechanoprotective influence of the
789 cytoskeleton reveals PIEZO1 is gated by bilayer tension. Nature Communications *7*.
790 Di Paolo, G., and De Camilli, P. (2006). Phosphoinositides in cell regulation and membrane dynamics.
791 Nature *443*, 651-657.
792 Dong, X.-p., Shen, D., Wang, X., Dawson, T., Li, X., Zhang, Q., Cheng, X., Zhang, Y., Weisman, L.S.,
793 Delling, M.*, et al.* (2010). PI(3,5)P2 Mucolipin Ca2+ Controls Membrane Traffic by Direct Activation
794 of Release Channels in the Endolysosome. Nature *1*, 1-21.
795 Dove, S.K., Cooke, F.T., Douglas, M.R., Sayers, L.G., Parker, P.J., and Michell, R.H. (1997). Osmotic
796 stress activates phosphatidylinositol-3,5-bisphosphate synthesis. Nature *390*, 187-192.
797 Drew, L.J., Rohrer, D.K., Price, M.P., Blaver, K.E., Cockayne, D.A., Cesare, P., and Wood, J.N. (2004).
798 Acid-sensing ion channels ASIC2 and ASIC3 do not contribute to mechanically activated currents in
799 mammalian sensory neurones. Journal of Physiology *556*, 691-710.
800 Dubin, A.E., Murthy, S., Lewis, A.H., Brosse, L., Cahalan, S.M., Grandl, J., Coste, B., and Patapoutian, A.
801 (2017). Endogenous Piezo1 Can Confound Mechanically Activated Channel Identification and
802 Characterization. Neuron *94*, 266-270.e263.
803 Dubin, A.E., Schmidt, M., Mathur, J., Petrus, M.J., Xiao, B., and Coste, B. (2012). Inflammatory Signals
804 Enhance Piezo2-Mediated Mechanosensitive Currents. CellReports *2*, 511-517.
805 Eijkelkamp, N., Linley, J.E., Torres, J.M., Bee, L., Dickenson, a.H., Gringhuis, M., Minett, M.S., Hong,
806 G.S., Lee, E., Oh, U.*, et al.* (2013). A role for Piezo2 in EPAC1-dependent mechanical allodynia.
807 Nature communications *4*, 1682.
808 Florez-Paz, D., Bali, K.K., Kuner, R., and Gomis, A. (2016). A critical role for Piezo2 channels in the
809 mechanotransduction of mouse proprioceptive neurons. Scientific Reports *6*, 25923.
810 Gamper, N., and Shapiro, M.S. (2007). Regulation of ion transport proteins by membrane
811 phosphoinositides. Nat Rev Neurosci *8*, 921-934.
812 Ge, J., Li, W., Zhao, Q., Li, N., Chen, M., Zhi, P., Li, R., Gao, N., Xiao, B., and Yang, M. (2015).
813 Architecture of the mammalian mechanosensitive Piezo1 channel. Nature *527*.
814 Guo, Y.R., and MacKinnon, R. (2017). Structure-based membrane dome mechanism for Piezo
815 mechanosensitivity. eLife *6*, e33660.
816 Hammond, G.R.V., Takasuga, S., Sasaki, T., and Balla, T. (2015). The ML1Nx2 phosphatidylinositol 3,5-
817 bisphosphate probe shows poor selectivity in cells. PLoS ONE *10*, 1-13.
818 Hanack, C., Moroni, M., Lima, W.C., Wende, H., Kirchner, M., Adelfinger, L., Schrenk-Siemens, K.,
819 Tappe-Theodor, A., Wetzel, C., Kuich, P.H.*, et al.* (2015). GABA blocks pathological but not acute
820 TRPV1 pain signals. Cell *160*, 759-770.
821 Ho, C.Y., Alghamdi, T.A., and Botelho, R.J. (2012). Phosphatidylinositol-3,5-bisphosphate: No longer
822 the poor PIP 2. Traffic *13*, 1-8.
823 Hu, J., Chiang, L.-Y., Koch, M., and Lewin, G.R. (2010). Evidence for a protein tether involved in
824 somatic touch. The EMBO journal *29*, 855-867.
825 Hu, J., and Lewin, G.R. (2006). Mechanosensitive currents in the neurites of cultured mouse sensory
826 neurones. The Journal of physiology *577*, 815-828.

827 Ikonomov, O.C., Sbrissa, D., Dondapati, R., and Shisheva, A. (2007). ArPIKfyve-PIKfyve interaction and
828 role in insulin-regulated GLUT4 translocation and glucose transport in 3T3-L1 adipocytes.
829 Experimental Cell Research *313*, 2404-2416.
830 Janmey, P.A. (1995). Protein regulation by phosphatidylinositol lipids. Chemistry and Biology *2*, 61-
831 65.
832 Jia, Z., Ikeda, R., Ling, J., Viatchenko-Karpinski, V., and Gu, J.G. (2016). Regulation of Piezo2
833 Mechanotransduction by Static Plasma Membrane Tension in Primary Afferent Neurons. J Biol
834 Chem *291*, 9087-9104.
835 Jin, N., Lang, M.J., and Weisman, L.S. (2016). Phosphatidylinositol 3,5-bisphosphate: regulation of
836 cellular events in space and time. Biochemical Society Transactions *44*, 177-184.
837 Kim, S.-A., Vacratsis, P.O., Firestein, R., Cleary, M.L., and Dixon, J.E. (2003). Regulation of
838 myotubularin-related (MTMR)2 phosphatidylinositol phosphatase by MTMR5, a catalytically
839 inactive phosphatase. Proceedings of the National Academy of Sciences of the United States of
840 America *100*, 4492-4497.
841 Klaus, F., Laufer, J., Czarkowski, K., Strutz-Seebohm, N., Seebohm, G., and Lang, F. (2009). PIKfyve-
842 dependent regulation of the Cl- channel ClC-2. Biochemical and Biophysical Research
843 Communications *381*, 407-411.
844 Laporte, J., Blondeau, F., Buj-Bello, A., Tentler, D., Kretz, C., Dahl, N., and Mandel, J.L. (1998).
845 Characterization of the myotubularin dual specificity phosphatase gene family from yeast to
846 human. Human Molecular Genetics *7*, 1703-1712.
847 Lechner, S.G., and Lewin, G.R. (2009). Peripheral sensitisation of nociceptors via G-protein-
848 dependent potentiation of mechanotransduction currents. The Journal of Physiology *587*, 3493-
849 3503.
850 Lechner, S.G., Markworth, S., Poole, K., Smith, E.S.J., Lapatsina, L., Frahm, S., May, M., Pischke, S.,
851 Suzuki, M., Ibanez-Tallon, I*., et al.* (2011). The molecular and cellular identity of peripheral
852 osmoreceptors. Neuron *69*, 332-344.
853 Lewis, A.H., and Grandl, J. (2015). Mechanical sensitivity of Piezo1 ion channels can be tuned by
854 cellular membrane tension. eLife *4*, 1-17.
855 Li, X., Garrity, A.G., and Xu, H. (2013a). Regulation of membrane trafficking by signalling on
856 endosomal and lysosomal membranes. The Journal of Physiology *591*, 4389-4401.
857 Li, X., Wang, X., Zhang, X., Zhao, M., Tsang, W.L., Zhang, Y., Yau, R.G.W., Weisman, L.S., and Xu, H.
858 (2013b). Genetically encoded fluorescent probe to visualize intracellular phosphatidylinositol 3,5-
859 bisphosphate localization and dynamics. Proceedings of the National Academy of Sciences of the
860 United States of America *110*, 21165-21170.
861 Liu, L., Chen, L., Liedtke, W., and Simon, S.a. (2007). Changes in osmolality sensitize the response to
862 capsaicin in trigeminal sensory neurons. Journal of neurophysiology *97*, 2001-2015.
863 Lou, S., Duan, B., Vong, L., Lowell, B.B., and Ma, Q. (2013). Runx1 controls terminal morphology and
864 mechanosensitivity of VGLUT3-expressing C-mechanoreceptors. The Journal of neuroscience : the
865 official journal of the Society for Neuroscience *33*, 870-882.
866 McCartney, A.J., Zhang, Y., and Weisman, L.S. (2014a). Phosphatidylinositol 3,5-bisphosphate: low
867 abundance, high significance. Bioessays *36*, 52-64.
868 McCartney, A.J., Zolov, S.N., Kauffman, E.J., Zhang, Y., Strunk, B.S., Weisman, L.S., and Sutton, M.A.
869 (2014b). Activity-dependent PI(3,5)P2 synthesis controls AMPA receptor trafficking during
870 synaptic depression. Proceedings of the National Academy of Sciences of the United States of
871 America *111*, E4896-4905.
872 McHugh, B.J., Buttery, R., Lad, Y., Banks, S., Haslett, C., and Sethi, T. (2010). Integrin activation by
873 Fam38A uses a novel mechanism of R-Ras targeting to the endoplasmic reticulum. Journal of Cell
874 Science *123*, 51-61.
875 Messenger, S.W., Thomas, D.D.H., Cooley, M.M., Jones, E.K., Falkowski, M.A., August, B.K.,
876 Fernandez, L.A., Gorelick, F.S., and Groblewski, G.E. (2015). Early to Late Endosome Trafficking
877 Controls Secretion and Zymogen Activation in Rodent and Human Pancreatic Acinar Cells. Cmgh *1*,
878 695-709.

879 Mironova, Y.A., Lenk, G.M., Lin, J.P., Lee, S.J., Twiss, J.L., Vaccari, I., Bolino, A., Havton, L.A., Min, S.H.,
880 Abrams, C.S*., et al.* (2016). PI(3,5)P2 biosynthesis regulates oligodendrocyte differentiation by
881 intrinsic and extrinsic mechanisms. eLife *5*, 1-29.
882 Mo, G., Bernier, L.-P., Zhao, Q., Chabot-Doré, A.-J., Ase, A.R., Logothetis, D., Cao, C.-Q., and Séguéla,
883 P. (2009). Subtype-Specific Regulation of P2X3 and P2X2/3 Receptors by Phosphoinositides in
884 Peripheral Nociceptors. Molecular Pain *5*, 1744-8069-1745-1747.
885 Morley, S.J., Qi, Y., Iovino, L., Andolfi, L., Guo, D., Kalebic, N., Castaldi, L., Tischer, C., Portulano, C.,
886 Bolasco, G*., et al.* (2016). Acetylated tubulin is essential for touch sensation in mice. eLife *5*, 25.
887 Narayanan, P., Sondermann, J., Rouwette, T., Karaca, S., Urlaub, H., Mitkovski, M., Gomez-Varela, D.,
888 and Schmidt, M. (2016). Native Piezo2 interactomics identifies pericentrin as a novel regulator of
889 Piezo2 in somatosensory neurons. Journal of Proteome Research *15*, 2676-2687.
890 Nawaz, S., Sa, P., Schmitt, S., Schaap, I.A.T., Lyons, D.A., and Velte, C. (2015). Actin Filament Turnover
891 Drives Leading Edge Growth during Myelin Sheath Formation in the Central Nervous System.
892 Developmental Cell *34*, 1-13.
893 Ng, A.A., Logan, A.M., Schmidt, E.J., and Robinson, F.L. (2013). The CMT4B disease-causing
894 phosphatases Mtmr2 and Mtmr13 localize to the Schwann cell cytoplasm and endomembrane
895 compartments, where they depend upon each other to achieve wild-type levels of protein
896 expression. Human Molecular Genetics *22*, 1493-1506.
897 Nicot, A.S., and Laporte, J. (2008). Endosomal phosphoinositides and human diseases. Traffic *9*, 1240-
898 1249.
899 Patapoutian, A., Tate, S., and Woolf, C.J. (2009). Transient receptor potential channels: targeting pain
900 at the source. Nature reviews Drug discovery *8*, 55-68.
901 Perozo, E., Cortes, D.M., Sompornpisut, P., Kloda, A., and Martinac, B. (2002). Open channel structure
902 of MscL and the gating mechanism of mechanosensitive channels. Nature *418*, 942-948.
903 Poole, K., Herget, R., Lapatsina, L., Ngo, H.-D., and Lewin, G.R. (2014). Tuning Piezo ion channels to
904 detect molecular-scale movements relevant for fine touch. Nature communications *5*, 3520.
905 Previtali, S.C., Quattrini, A., and Bolino, A. (2007). Charcot-Marie-Tooth type 4B demyelinating
906 neuropathy: deciphering the role of MTMR phosphatases. Expert reviews in molecular medicine
907 *9*, 1-16.
908 Previtali, S.C., Zerega, B., Sherman, D.L., Brophy, P.J., Dina, G., King, R.H.M., Salih, M.M., Feltri, L.,
909 Quattrini, A., Ravazzolo, R*., et al.* (2003). Myotubularin-related 2 protein phosphatase and
910 neurofilament light chain protein, both mutated in CMT neuropathies, interact in peripheral
911 nerve. Human Molecular Genetics *12*, 1713-1723.
912 Qi, Y., Andolfi, L., Frattini, F., Mayer, F., Lazzarino, M., and Hu, J. (2015). Membrane stiffening by
913 STOML3 facilitates mechanosensation in sensory neurons. Nature Communications *6*, 8512.
914 Quallo, T., Vastani, N., Horridge, E., Gentry, C., Parra, A., Moss, S., Viana, F., Belmonte, C., Andersson,
915 D.a., and Bevan, S. (2015). TRPM8 is a neuronal osmosensor that regulates eye blinking in mice.
916 Nature Communications *6*, 7150.
917 Ranade, S.S., Woo, S.-H., Dubin, A.E., Moshourab, R.a., Wetzel, C., Petrus, M., Mathur, J., Bégay, V.,
918 Coste, B., Mainquist, J*., et al.* (2014). Piezo2 is the major transducer of mechanical forces for
919 touch sensation in mice. Nature *516*, 121-125.
920 Raucher, D., Stauffer, T., Chen, W., Shen, K., Guo, S., York, J.D., Sheetz, M.P., and Meyer, T. (2000).
921 Phosphatidylinositol 4,5-Bisphosphate Functions as a Second Messenger that Regulates
922 Cytoskeleton–Plasma Membrane Adhesion. Cell *100*, 221-228.
923 Rehfeldt, F., Engler, A.J., Eckhardt, A., Ahmed, F., and Discher, D.E. (2007). Cell responses to the
924 mechanochemical microenvironment— Implications for regenerative medicine and drug delivery.
925 Advanced Drug Delivery Reviews *59*, 1329-1339.
926 Robinson, F.L., and Dixon, J.E. (2005). The phosphoinositide-3-phosphatase MTMR2 associates with
927 MTMR13, a membrane-associated pseudophosphatase also mutated in type 4B Charcot-Marie-
928 Tooth disease. Journal of Biological Chemistry *280*, 31699-31707.
929 Saotome, K., Murthy, S.E., Kefauver, J.M., Whitwam, T., Patapoutian, A., and Ward, A.B. (2017).
930 Structure of the mechanically activated ion channel Piezo1. Nature, 1-23.

Schindelin, J., Rueden, C.T., Hiner, M.C., and Eliceiri, K.W. (2015). The ImageJ ecosystem: An open platform for biomedical image analysis. Molecular Reproduction and Development *82*, 518-529.
Skwarekmaruszewska, a., Hotulainen, P., and Lappalainen, P. (2006). Regulation of the Actin Cytoskeleton by Phospholipids. Advances in Molecular and Cell Biology *37*, 201-219.
Sukharev, S. (2002). Purification of the small mechanosensitive channel of Escherichia coli (MscS): the subunit structure, conduction, and gating characteristics in liposomes. Biophysical journal *83*, 290-298.
Szczot, M., Pogorzala, L.A., Solinski, H.J., Young, L., Yee, P., Le Pichon, C.E., Chesler, A.T., and Hoon, M.A. (2017). Cell-Type-Specific Splicing of Piezo2 Regulates Mechanotransduction. Cell Reports *21*, 2760-2771.
Tsuruta, F., Green, E.M., Rousset, M., and Dolmetsch, R.E. (2009). PIKfyve regulates CaV1.2 degradation and prevents excitotoxic cell death. Journal of Cell Biology *187*, 279-294.
Vaccari, I., Dina, G., Tronchere, H.l.n., Kaufman, E., Chicanne, G.t., Cerri, F., Wrabetz, L., Payrastre, B., Quattrini, A., Weisman, L.S*., et al.* (2011). Genetic interaction between MTMR2 and FIG4 phospholipid phosphatases involved in Charcot-Marie-Tooth neuropathies. PLoS Genetics *7*.
Vásquez, V., Krieg, M., Lockhead, D., and Goodman, M.B. (2014). Phospholipids that Contain Polyunsaturated Fatty Acids Enhance Neuronal Cell Mechanics and Touch Sensation. Cell Reports *6*, 70-80.
Viatchenko-Karpinski, V., and Gu, J.G. (2016). Mechanical sensitivity and electrophysiological properties of acutely dissociated dorsal root ganglion neurons of rats. Neuroscience Letters *634*, 70-75.
Wetzel, C., Hu, J., Riethmacher, D., Benckendorff, A., Harder, L., Eilers, A., Moshourab, R., Kozlenkov, A., Labuz, D., Caspani, O*., et al.* (2007). A stomatin-domain protein essential for touch sensation in the mouse. Nature *445*, 206-209.
Woo, S.-H., Lukacs, V., de Nooij, J.C., Zaytseva, D., Criddle, C.R., Francisco, A., Jessell, T.M., Wilkinson, K.a., and Patapoutian, A. (2015). Piezo2 is the principal mechanotransduction channel for proprioception. Nature Neuroscience, 1-8.
Woo, S.-H., Ranade, S., Weyer, A.D., Dubin, A.E., Baba, Y., Qiu, Z., Petrus, M., Miyamoto, T., Reddy, K., Lumpkin, E.a*., et al.* (2014). Piezo2 is required for Merkel-cell mechanotransduction. Nature *509*, 622-626.
Wu, J., Goyal, R., Grandl, J., Coste, B., Coste, B., Coste, B., Ge, J., Li, J., Woo, S.H., Maksimovic, S*., et al.* (2016a). Localized force application reveals mechanically sensitive domains of Piezo1. Nature Communications *7*.
Wu, J., Lewis, A.H., and Grandl, J. (2016b). Touch, Tension, and Transduction – The Function and Regulation of Piezo Ion Channels. Trends in Biochemical Sciences *42*.
Yan, Y., and Backer, J.M. (2007). Regulation of class III (Vps34) PI3Ks. Biochemical Society transactions *35*, 239-241.
Zhang, Y., McCartney, A.J., Zolov, S.N., Ferguson, C.J., Meisler, M.H., Sutton, M.a., and Weisman, L.S. (2012). Modulation of synaptic function by VAC14, a protein that regulates the phosphoinositides PI(3,5)P2 and PI(5)P. The EMBO Journal *31*, 3442-3456.
Zolov, S.N., Bridges, D., Zhang, Y., Lee, W.-w., Riehle, E., Verma, R., and Lenk, G.M. (2012). In vivo, Pikfyve generates PI(3,5)P2, which serves as both a signaling lipid and the major precursor for PI5P. Proceedings of the National Academy of Sciences *109*, 17472-17477.

Figure Legends

Figure 1: Mtmr2 suppresses Piezo2-mediated RA-MA currents in HEK293 cells and DRG neurons

(a-d) Representative images **(a,c)** and quantification **(b,d)** of a proximity ligation assay (PLA) in cultured DRG neurons (a,b) of *Piezo2*^{GFP} mice (Woo et al., 2014) and HEK293 cells (c,d). As anti-Mtmr2 antibodies fail to work in neuronal cultures, DRG were transfected with Mtmr2-myc or mock-

myc and PLA was performed with antibodies against Piezo2 and myc. Please note the distribution of the PLA signal in soma and neurites of DRG. HEK293 cells were co-transfected with Piezo2-GST-IRES-GFP and Mtmr2-myc or Piezo2-GST-IRES-GFP and mock-myc and PLA was performed with antibodies against GST and myc. Only cell types with pronounced GFP signal (due to expression of pmaxGFP®Vector in DRG and Piezo2-GST-IRES-GFP in HEK293 cells) were considered for the analysis. Cell boundaries are demarcated in yellow. In both cell types transfection of Mtmr2-myc exhibited significantly stronger PLA signal in somata and neurites (of DRG neurons) compared to controls **(b,d).** Scale bar: 10 µm. Quantification of the total area of PLA signal/total soma area (fraction of PLA-positive area) in DRG cultures ($p < 0.0001$; Mann-Whitney test; + mock: n = 53 neurons; + Mtmr2-myc: n = 53 neurons) **(b)**. The quantification of the intensity of PLA signal in neurites of cultured DRG neurons can be found in Supplemental Figure 1c. Quantification of the total area of PLA signal/total cell area in HEK293 cells (fraction of PLA-positive area) ($p < 0.0001$; Mann-Whitney test; Piezo2-GST + mock: n = 60 cells; Piezo2-GST + Mtmr2-myc: n = 54 cells) **(d).** Additional controls for PLA in HEK293 cells can be found in Supplemental Figure 1d. **(e)** Representative traces of RA-MA currents in HEK293 cells upon co-expression of Piezo2 with mock or Mtmr2 and **(f)** stimulus-current curves. Overexpression of Mtmr2 suppressed Piezo2 current magnitudes compared to mock overexpression (Piezo2 + mock: n = 17 cells; Piezo2 + Mtmr2: n = 12 cells; 2-way ANOVA suggested a significant effect ($P < 0.0001$) of Mtmr2 overexpression on Piezo2 currents; Holm-Sidak's multiple comparisons test was used to compare both conditions at individual stimulus magnitudes, p-values are indicated by * in the graph). The displacement threshold was increased upon co-expression of Mtmr2 ($p = 0.0098$; Mann-Whitney test; Supplementary File 1). The inactivation time constant of RA-MA currents remained unchanged (Supplementary File 1). **(g)** Representative traces of RA-MA currents in primary cultures of DRG neurons and **(h)** stimulus-current curves showed a significant decrease in RA-MA current magnitude upon overexpression of Mtmr2 compared to mock (+ mock: n = 28 neurons; + Mtmr2: n = 30 neurons; 2-way ANOVA suggested a significant effect ($P < 0.0022$) of Mtmr2 overexpression on RA-MA currents; Holm-Sidak's multiple comparison test was performed to compare both conditions at individual stimulus magnitudes, p-values are indicated by * in the graph). The displacement threshold and inactivation time constant of RA-MA currents were not changed upon overexpression of Mtmr2 in DRG neurons (Supplementary File 1).

Figure 1-figure supplement 1: Mtmr2 is expressed in mouse DRG and partially overlaps with Piezo2

(a) Representative immunohistochemistry and **(b)** quantification of Mtmr2-positive neurons in cryosections of DRGs obtained from Piezo2^{GFP} mice (Woo et al., 2014). 20.37 ± 2.01% of DRG neurons exhibit positive Mtmr2 immunolabel and 24.53 ± 1.21% of DRG neurons were positive for GFP indicating the presence of Piezo2. Among Piezo2-positive cells, 51.61 ± 3.71% cells were found to be Mtmr2-positive. n > 2000 neurons, N = 3 independent animals. **(c)** Quantification of the intensity of PLA signal in neurites of cultured DRG neurons ($p < 0.0001$ compared to + mock, Mann Whitney test; + mock: n = 94 regions from 6 coverslips; + Mtmr2-myc: n = 115 regions from 6 coverslips. **(d)** Quantification of PLA signal upon co-expression of Piezo2 with mock, Mtmr2, Vti1b (Vesicle transport through interaction with t-SNAREs homolog 1B) or TRPA1 in HEK293 cells. PLA was performed using antibodies against GST and myc to detect Piezo2-GST-IRES-GFP and myc-tagged proteins, respectively. PLA signal (fraction of PLA-positive area) upon co-transfection of mock, Vti1b and TRPA1 served as negative controls and was indeed much smaller than the PLA signal upon co-transfection of Piezo2 and Mtmr2 ($p < 0.01$, in case of TRPA1 $p=0.052$ compared to Piezo2 + Mtmr2, Kruskal-Wallis

test followed by Dunn´s multiple comparison test; Piezo2-GST + mock: n = 60 cells; Piezo2-GST + Mtmr2-myc: n = 35 cells; Piezo2-GST + Vti1b-myc: n = 54 cells; Piezo2-GST + TRPA1-myc: n = 83 cells). Only cells with pronounced GFP signal (due to expression of Piezo2-GST-IRES-GFP) were considered for the analysis. All experiments were performed in parallel.

Figure 1-figure supplement 2: Mtmr2 overexpression does not influence Kv1.1- or Piezo1-mediated currents

(a) Voltage-current curves upon overexpression of Kv1.1 with Mtmr2 in HEK293 cells showed no significant difference compared to overexpression with mock (Kv1.1 + mock: n = 24 cells; Kv1.1 + Mtmr2: n = 25 cells; ns; 2-way ANOVA). **(b)** Stimulus-current curves of Piezo1-mediated MA currents upon co-overexpression of Piezo1 (Piezo1-753-myc-IRES-GFP (Coste et al., 2015)) with Mtmr2 compared to mock. No significant difference was observed among conditions (Piezo1 + mock: n = 25 cells; Piezo1 + Mtmr2: n = 20 cells; ns; 2-way ANOVA). The displacement threshold and inactivation time constant of Piezo1-MA currents remained unchanged upon overexpression with Mtmr2 (Supplementary File 1).

Figure 2: Mtmr2 knockdown potentiates Piezo2 activity in peripheral sensory neurons
(a) Representative traces of RA-MA currents in primary cultures of DRG neurons and **(b)** stimulus-current curves for RA-MA currents upon nucleofection of *Mtmr2* siRNA showed a significant increase in RA-MA current magnitude compared to nucleofection with AllStar Negative Control siRNA (CTRL: n = 66 neurons; *Mtmr2* siRNA: n = 77 neurons; 2-way ANOVA suggested a pronounced effect ($P < 0.0003$) of Mtmr2 knockdown on RA-MA currents; Holm-Sidak's multiple comparisons test was used to compare both conditions at individual stimulus magnitudes, p-values are indicated by * in the graph). The displacement threshold and inactivation time constant of RA-MA currents remained unchanged upon knockdown of Mtmr2 (Supplementary File 1). Of note, MA current properties cannot be compared between different experiments or treatments of DRG cultures, e.g. Figure 2b cannot be compared to overexpression of Mtmr2 (Figure 1). Cultures were differently nucleofected (siRNA vs. plasmids) and recorded on different days in vitro (DIV) according to established protocols (please see Methods for details). Hence matching controls were performed for each set of data. **(c)** Stimulus-current curves show IA-MA currents were unaffected by knockdown of Mtmr2 in DRG neurons (CTRL: n = 23 neurons; *Mtmr2* siRNA: n = 10 neurons; ns; 2-way ANOVA). **(d)** Stimulus-current curves show SA-MA currents were unchanged upon Mtmr2 knockdown (n = 11-12 neurons per condition; ns; 2-way ANOVA). Of note, the displacement thresholds and inactivation time constants of IA-MA and SA-MA currents remained unchanged upon *Mtmr2* siRNA nucleofection (Supplementary File 1). **(e)** Stacked histograms show the number of cells exhibiting different MA currents upon knockdown of Mtmr2 in cultured DRG. The proportions of cells exhibiting RA and IA currents were significantly changed in cultures transfected with *Mtmr2* siRNA. RA:IA:SA:NR (% of total; rounded to whole numbers): CTRL: 46:16:9:29; *Mtmr2* siRNA: 58:7:12:23; $p < 0.044$ overall and for the proportion of RA/total ($p = 0.048$) and IA/total ($p = 0.023$), respectively; Chi-square test; ≥ 130 neurons were analyzed per condition). NR (non-responsive), refers to cells which showed no MA current.

Figure 2-figure supplement 1: Mtmr2 knockdown in cultured DRG neither affects Piezo2 mRNA nor Piezo2 membrane levels or overall expression

(a) Quantification of *Mtmr2* mRNA upon siRNA transfection in DRG neurons showed a significant decrease in *Mtmr2* mRNA (Actin as reference: 0.42 ± 0.05; $p < 0.0001$; one sample t-test; N = 8 independent DRG cultures). Of note, our qPCR results indicate successful siRNA-mediated knockdown of *Mtmr2* across the whole coverslip, which also includes non-transfected neurons and glia cells. Therefore our data do not report on the transfection efficiency and extent of Mtmr2 knockdown in individual neurons. **(b)** Quantification of *Piezo2* mRNA upon Mtmr2 knockdown in DRG neurons confirmed that *Piezo2* mRNA levels are similar to controls (*Actin* (*Actb*) as reference: 1.17 ± 0.18; ns; one sample t-test; N = 8 independent DRG cultures). **(c)** Quantification of Piezo2 membrane expression in DRG cultures derived from Piezo2^{GFP} mice (Woo et al., 2014) upon Mtmr2 knockdown. No difference was observed among conditions (CTRL: 1470 ± 246.7 AU; *Mtmr2* siRNA: 1424 ± 237.5 AU; n = 22 neurons per condition from N = 2 independent DRG cultures; ns; Mann-Whitney test). AU, arbitrary units. **(d)** Percentage of Piezo2-positive cells in DRG cultures derived from Piezo2^{GFP} mice treated with CTRL or *Mtmr2* siRNA. No difference was observed among analyzed conditions (CTRL: 29.59 ± 4.97%; *Mtmr2* siRNA: 33.59 ± 2.45%; ns; Mann-Whitney test; n > 1000 neurons per condition; N = 3 independent DRG cultures).

Figure 3: Catalytic activity of Mtmr2 is necessary to suppress Piezo2-mediated RA-MA currents

(a) Stimulus-current curves upon co-expression of Piezo2 with the catalytically inactive Mtmr2 C417S mutant in HEK293 cells compared to mock controls. Mtmr2 C417S overexpression slightly, but not significantly increased Piezo2 RA-MA currents especially at lower stimulus magnitudes (Piezo2 + mock: n = 17 cells; Piezo2 + Mtmr2 C417S: n = 18 cells). 2-way ANOVA reported a significant ($P < 0.0021$) overall effect of Mtmr2 C417S overexpression on RA-MA currents, however a Holm-Sidak's multiple comparisons test showed no significant difference between currents at individual stimulus magnitudes.). Of note, the displacement thresholds and inactivation time constant were unaffected upon overexpression with Mtmr2 C417S compared to mock (Supplementary File 1). **(b-c)** Representative images **(b)** and quantification **(c)** of PLA signal using antibodies against GST and myc to detect Piezo2-GST-IRES-GFP and Mtmr2 C417S-myc, respectively. PLA signal upon co-transfection of Piezo2-GST + Mtmr2 C417S-myc was indistinguishable from Piezo2-GST + Mtmr2-myc and significantly stronger than Piezo2-GST + mock. Cell boundaries are demarcated in yellow. Only cells with pronounced GFP signal (due to expression of Piezo2-GST-IRES-GFP) were considered for the analysis. Scale bar: 10 µm. Quantification of the number of the total area of PLA signal/total cell area (fraction of PLA-positive area) **(c)**; $p < 0.0001$ compared to Piezo2-GST + mock, Kruskal-Wallis test followed by Dunn's Multiple Comparison Test; Piezo2-GST + mock: n = 75 cells; Piezo2-GST + Mtmr2-myc: n = 70 cells; Piezo2-GST + Mtmr2 C417S-myc: n = 70 cells.

Figure 4: Mtmr2 modulates Piezo2-mediated RA-MA currents mainly via PI(3,5)P_2

(a) Scheme illustrating the major steps of PI(3,5)P_2 synthesis and turnover including commonly used inhibitors and their targets. Wortmannin is an inhibitor of the phosphatidylinositol 3-kinase (PI3-Kinase) while Apilimod inhibits phosphatidylinositol 3-phosphate 5-kinase (PIKfyve). Fig4 protein is a polyphosphoinositide phosphatase. **(b)** Stimulus-current curves after addition of Wortmannin, Apilimod or vehicle (DMSO) to *Mtmr2* siRNA-treated neurons (*Mtmr2* siRNA + DMSO: n = 27 neurons; *Mtmr2* siRNA + Wortmannin: n = 28 neurons; *Mtmr2* siRNA + Apilimod: n = 30 neurons). 2-way ANOVA suggested a significant ($P < 0.0007$) overall effect on RA-MA currents. Holm-Sidak's multiple comparisons test was performed to compare both conditions to DMSO at individual stimulus

magnitudes. While no significant difference between Wortmannin and DMSO at individual stimulus magnitudes was observed, Apilimod application showed a significant reduction of currents compared to DMSO, p-values are indicated by * in the graph. Similarly, only Apilimod treatment increased the displacement threshold (p = 0.0055 compared to DMSO-treated neurons, Kruskal-Wallis test followed by Dunn´s multiple comparisons test; Supplementary File 1). The inactivation time constants were unaltered by either treatment (Supplementary File 1). **(c)** Hypotonic extracellular solution counteracted the inhibition of Piezo2 RA-MA currents caused by Mtmr2 overexpression. Stimulus-current curves for Piezo2 RA-MA currents upon extracellular hypotonic stress application to DRG neurons overexpressing Mtmr2 (Mtmr2 + Isotonic extracellular solution: n = 14 neurons; Mtmr2 + Hypotonic extracellular solution: n = 19 neurons; 2-way ANOVA suggested that extracellular hypotonic stress had a significant (P < 0.0001) effect on RA-MA currents. Holm-Sidak's multiple comparisons test was performed to compare both conditions at individual stimulus magnitudes, p-values are indicated by * in the graph. The displacement threshold of RA-MA currents and inactivation time constant of RA-MA currents were unchanged (Supplementary File 1). **(d)** Hypotonic intracellular solution counteracted the potentiation of Piezo2 RA-MA currents caused by Mtmr2 knockdown. Stimulus-current curves for Piezo2 RA-MA currents upon intracellular hypotonic stress application to DRG neurons treated with *Mtmr2* siRNA (*Mtmr2* siRNA + Isotonic intracellular solution: n = 29 neurons; *Mtmr2* siRNA + Hypotonic intracellular solution: n = 25 neurons; 2-way ANOVA suggested that intracellular hypotonic stress had a significant (P < 0.0001) effect on RA-MA currents. Holm-Sidak's multiple comparisons test was performed to compare both conditions at individual stimulus magnitudes, p-values are indicated by * in the graph. The displacement threshold of RA-MA currents was increased upon intracellular hypotonic stress (p = 0.0131; Mann-Whitney test; Supplementary File 1). The inactivation time constant of RA-MA currents was unchanged (Supplementary File 1).

Figure 4-figure supplement 1: Effect on Piezo2 RA-MA currents upon application of PIPs or Apilimod in cultured DRG

(a) Stimulus-current curves of RA-MA currents are not altered upon addition of 1µM PI(3)P or 1µM $PI(3,5)P_2$ (CTRL: n = 27 neurons; 1µM PI(3)P: n = 17 neurons; 1µM $PI(3,5)P_2$: n = 21 neurons; ns; 2-way ANOVA). The displacement threshold and inactivation time constant of RA-MA currents also remained unchanged upon application of PIPs (Supplementary File 1). **(b)** Stimulus-current curves of RA-MA currents upon application of Apilimod or DMSO (vehicle) to wild type, untreated DRG neurons (+DMSO: n = 16 neurons; + Apilimod: n = 12 neurons; ns; 2-way ANOVA). The displacement threshold and inactivation time constant (τ) of RA-MA currents remained unchanged upon treatment with Apilimod (Supplementary File 1). **(c)** Stimulus-current curves demonstrate Piezo2 RA-MA potentiation upon application of extracellular hypotonic stress to DRG cultures compared to isotonic conditions (Isotonic extracellular: n = 53 neurons; Hypotonic extracellular: n = 81 neurons). 2-way ANOVA suggested that hypotonic stress had a significant (P < 0.0001) effect on RA-MA currents. Holm-Sidak's multiple comparisons test was performed to compare conditions at individual stimulus magnitudes, p-values are indicated by * in the graph. The displacement threshold of RA-MA currents was significantly decreased by hypotonic stress (p=0.0021; Mann-Whitney test; Supplementary File 1). Given that Jia and colleagues (Jia et al., 2016) reported slower inactivation of MA currents upon prolonged hypotonic stress, we wanted to ensure that measured currents in our paradigm of acute hypotonic stress were of the RA-type. In fact, this was the case as judged by comparable inactivation time constants (Supplementary File 1). Of note, MA current properties shown here in wild type,

untreated DRG neurons cannot be compared to nucleofected neurons in Figure 4. Nucleofection with siRNA or plasmids (i) alters neuronal and Piezo2 activity and (ii) required recordings to be performed on different days in vitro (2 DIV and 3 DIV, respectively) according to established protocols. Please see Methods for more details on variability in DRG cultures. For this reason each dataset consists of experiments and respective matching controls measured in parallel (i) in the same mouse cohort and (ii), where possible, on each experimental day.

Figure 4-figure supplement 2: Mtmr2 knockdown does not obviously alter mechanical properties of cultured DRG neurons

(a) Sketch of the AFM set-up used to measure the mechanical properties of cultured DRG neurons transfected with CTRL or *Mtmr2* siRNA. **(b)** Representative force-indentation curves for CTRL and *Mtmr2* siRNA treated DRG neurons. **(c)** Quantification of effective Young' modulus (E_{eff}) of DRG neurons shows no significant difference between CTRL and *Mtmr2* siRNA treatment (CTRL: 0.93 ± 0.13 kPa, n = 44 neurons from N = 4 independent cultures; *Mtmr2* siRNA: 0.96 ± 0.09 kPa, n = 48 neurons from N = 4 independent cultures; ns; Mann-Whitney test). **(d)** Quantification of tether force also showed no difference between conditions (37.74 ± 0.55 pN, n = 53 from N = 4 independent cultures; *Mtmr2* siRNA: 38.30 ± 0.76 pN, n = 54 from N = 4 independent cultures; ns; Mann-Whitney test).

Figure 5: Murine Piezo2, but not Piezo1, harbors a PIP_2 binding motif

(a) Schematic view of the $PI(3,5)P_2$ binding region of TRPML1 identified elsewhere (Dong et al., 2010) and the region in murine Piezo2 that exhibits pronounced sequence similarity to the $PI(3,5)P_2$ binding region of TRPML1. The indicated sequences were used to generate peptides for Piezo2, the Piezo2 3Q mutant and Piezo1. All peptides were tagged with a FLAG-epitope to allow for detection with anti-Flag antibodies on immunoblots. **(b-d)** Representative peptide-lipid binding assays followed by immunoblotting after incubation with indicated peptides (**b, c**) and densitometric quantification (**d**). The arrangement of lipids on the lipid-strip is indicated; blank, no lipid was spotted. The Piezo2 peptide strongly binds to $PI(3,5)P_2$ and $PI(4,5)P_2$, and weakly to $PI(3,4)P_2$. Neither the Piezo2 3Q mutant peptide nor the Piezo1 peptide exhibited significant binding to any of the lipids tested. One-way ANOVA followed by Dunnett's multiple comparisons test was used to compare spot signal densities for each peptide to the respective blank, p-values are indicated by # in the graph (**d**). In addition, one-way ANOVA followed by Holm-Sidak's multiple comparisons test was used to compare spot signal densities across the three peptides, p-values are indicated by * in the graph (**d**). The graph only presents data for those lipids to which the Piezo2 peptide exhibited significant binding. Please see Figure 5-figure supplement 1 for summarized data on lipids tested with the Piezo2 peptide. Experiments using the Piezo2 peptides were independently repeated 6 times of which 4 times were conducted in parallel with experiments using the Piezo1 peptide. AU, arbitrary units. **(e)** Stimulus-current curves upon co-expression of the Piezo2 P1 mutant with Mtmr2 in HEK293 cells compared to mock controls. Mtmr2 only slightly attenuated MA currents (Piezo2 P1 mutant + mock: n = 13 cells; Piezo2 P1 mutant + Mtmr2: n = 10 cells). 2-way ANOVA reported a significant ($P < 0.0119$) overall effect of Mtmr2 overexpression on RA-MA currents of the Piezo2 P1 mutant, however a Holm-Sidak's multiple comparisons test showed no significant difference between currents at individual stimulus magnitudes. Of note, the displacement threshold and inactivation time constant were also unaffected upon overexpression of Mtmr2 compared to mock (Supplementary File 1).

Figure 5-figure supplement 1: Quantification of peptide-lipid binding assays using the Piezo2 peptide

Piezo2 peptide densitometry data were analyzed using one-way ANOVA followed by Dunnett's multiple comparisons test to compare spot signal densities for different lipids to the blank, p-values are indicated by # in the graph. AU, arbitrary units.

Figure 6: Working model: Local control of Piezo2 function by interdependent actions of Mtmr2 and PI(3,5)P_2

Mtmr2 controls the abundance of PI(3,5)P_2 by dephosphorylation (please see Figure 4a). Mtmr2 and Piezo2 expression as well as PI(3,5)P_2 might be compartmentalized in membrane microdomains. Piezo2 localization in Mtmr2-negative microdomains would facilitate its access to local PI(3,5)P_2 and consequently potentiate Piezo2 RA-MA currents (left side). On the other hand, high Mtmr2 levels and its localization in the proximity of Piezo2 would augment PI(3,5)P_2 turnover, thereby decreasing local PI(3,5)P_2 availability and suppressing Piezo2 RA-MA currents (right side). One could further speculate that Mtmr2, via binding Piezo2, might recruit Piezo2 to membrane microdomains depleted of PI(3,5)P_2. This would provide an active mechanism to inhibit Piezo2 RA-MA currents in membrane compartments – may they be at the plasma membrane or intracellular membranes. Ultimately, Mtmr2 and PI(3,5)P_2 may contribute to dynamically tuning touch sensitivity of an organism in response to diverse conditions modulating Mtmr2 and PI(3,5)P_2 levels (e.g. osmotic stress as indicated by results shown in Figure 4).The following questions await further clarification: (i) How are Mtmr2/PI(3,5)P_2 regulated during (patho)physiological conditions in the somatosensory system, (ii) does the modulation of RA-MA currents require additional yet to be identified effector proteins, and (iii) are other PIPs also involved, e.g. PI(4,5)P_2 shown to modulate Piezo2 function (Borbiro et al., 2015)? As the structure of Piezo2 has not been resolved yet, Piezo2 is depicted after the recently solved structure of Piezo1 (Ge et al., 2015; Guo and MacKinnon, 2017; Saotome et al., 2017). If this structure holds true for Piezo2, the PI(3,5)P_2 binding domain (depicted in green) would roughly be localized within the first third of the N-terminal blade.

Supplementary File 1: Summary of properties of MA currents elicited under various conditions in HEK293 cells and DRG neurons

The table shows the displacement threshold and inactivation time constant (τ) values for all electrophysiological data presented in this study (please see Methods for details on the calculation of each value). Values are represented as mean ± SEM and cell numbers are indicated by 'n'. Data were not significant (ns) unless otherwise mentioned. Please note: for SA-MA currents, it was not possible to fit the current traces of all cells with a mono or bi-exponential fit (please see methods for details), hence the cell numbers measured for the inactivation time constant (τ) are lower than actual cell numbers measured and reported in Figure 2.

Figure 1

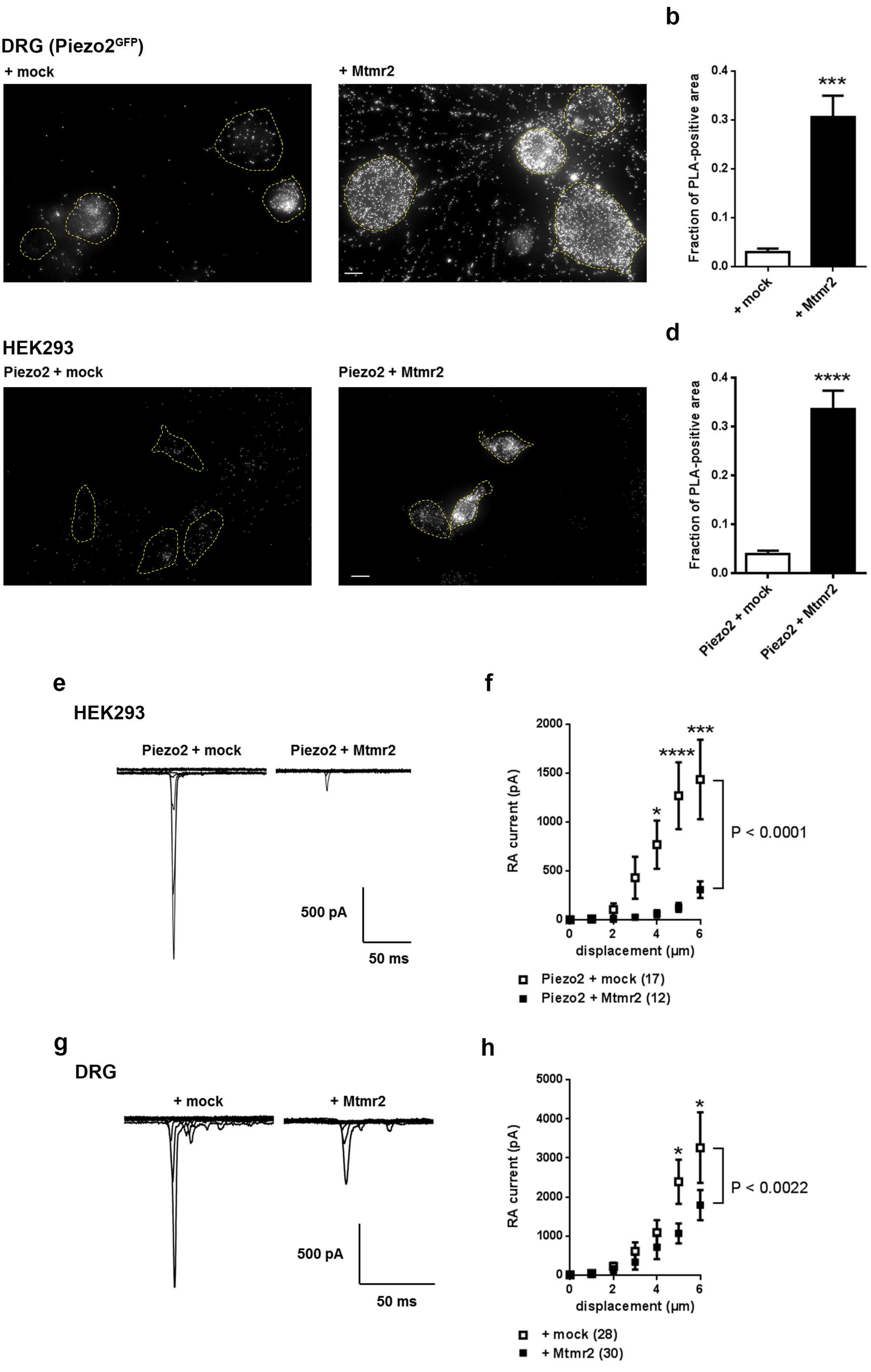
a
DRG (Piezo2GFP)
+ mock
+ Mtmr2
b
Fraction of PLA-positive area
0.4
0.3
0.2
0.1
0.0
***
+ mock
+ Mtmr2
c
HEK293
Piezo2 + mock
Piezo2 + Mtmr2
d
Fraction of PLA-positive area
0.4
0.3
0.2
0.1
0.0
****
Piezo2 + mock
Piezo2 + Mtmr2
e
HEK293
Piezo2 + mock
Piezo2 + Mtmr2
500 pA
50 ms
f
RA current (pA)
2000
1500
1000
500
0
0
2
4
6
displacement (µm)
*
****
***
P < 0.0001
Piezo2 + mock (17)
Piezo2 + Mtmr2 (12)
g
DRG
+ mock
+ Mtmr2
500 pA
50 ms
h
RA current (pA)
5000
4000
3000
2000
1000
0
0
2
4
6
displacement (µm)
*
*
P < 0.0022
+ mock (28)
+ Mtmr2 (30)

Figure 2

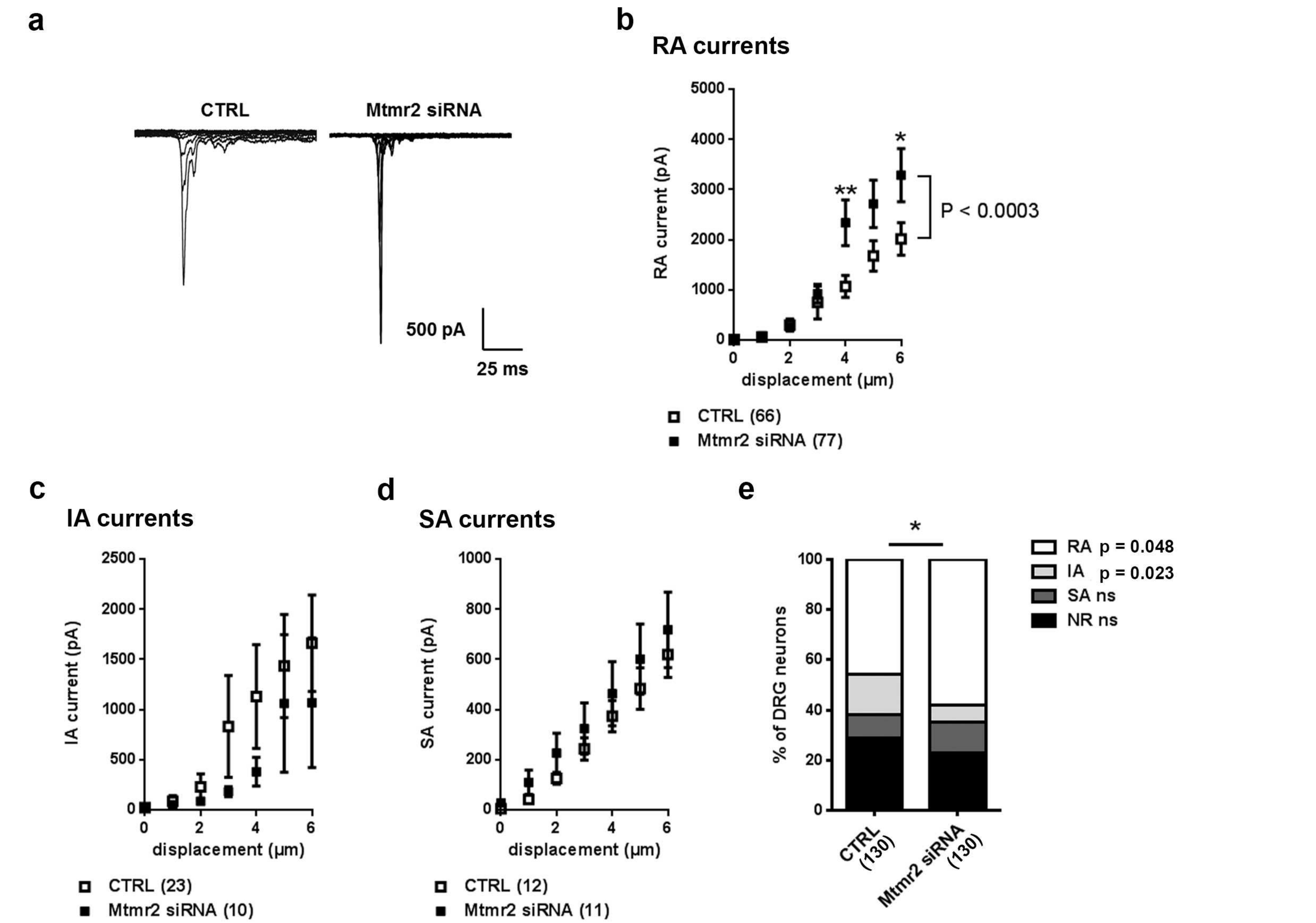
a
CTRL
Mtmr2 siRNA
500 pA
25 ms
b
RA currents
RA current (pA)
5000
4000
3000
2000
1000
0
**
*
P < 0.0003
0
2
4
6
displacement (µm)
CTRL (66)
Mtmr2 siRNA (77)
c
IA currents
IA current (pA)
2500
2000
1500
1000
500
0
displacement (µm)
CTRL (23)
Mtmr2 siRNA (10)
d
SA currents
SA current (pA)
1000
800
600
400
200
0
displacement (µm)
CTRL (12)
Mtmr2 siRNA (11)
e
*
% of DRG neurons
100
80
60
40
20
0
RA p = 0.048
IA p = 0.023
SA ns
NR ns
CTRL (130)
Mtmr2 siRNA (130)

Figure 3

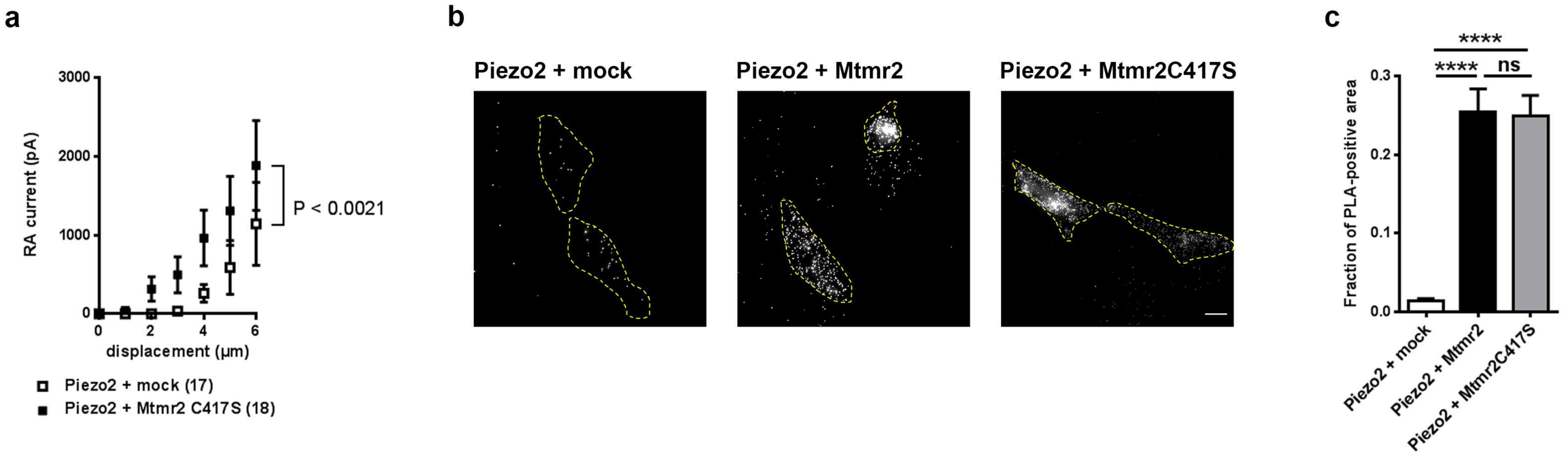
a
3000
2000
1000
0
RA current (pA)
0
2
4
6
displacement (µm)
P < 0.0021
Piezo2 + mock (17)
Piezo2 + Mtmr2 C417S (18)
b
Piezo2 + mock
Piezo2 + Mtmr2
Piezo2 + Mtmr2C417S
c
****
****
ns
0.3
0.2
0.1
0.0
Fraction of PLA-positive area
Piezo2 + mock
Piezo2 + Mtmr2
Piezo2 + Mtmr2C417S

Figure 4

a

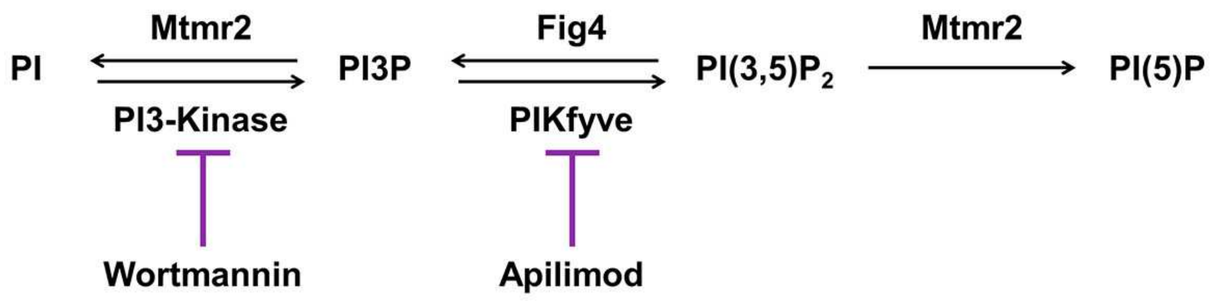

b

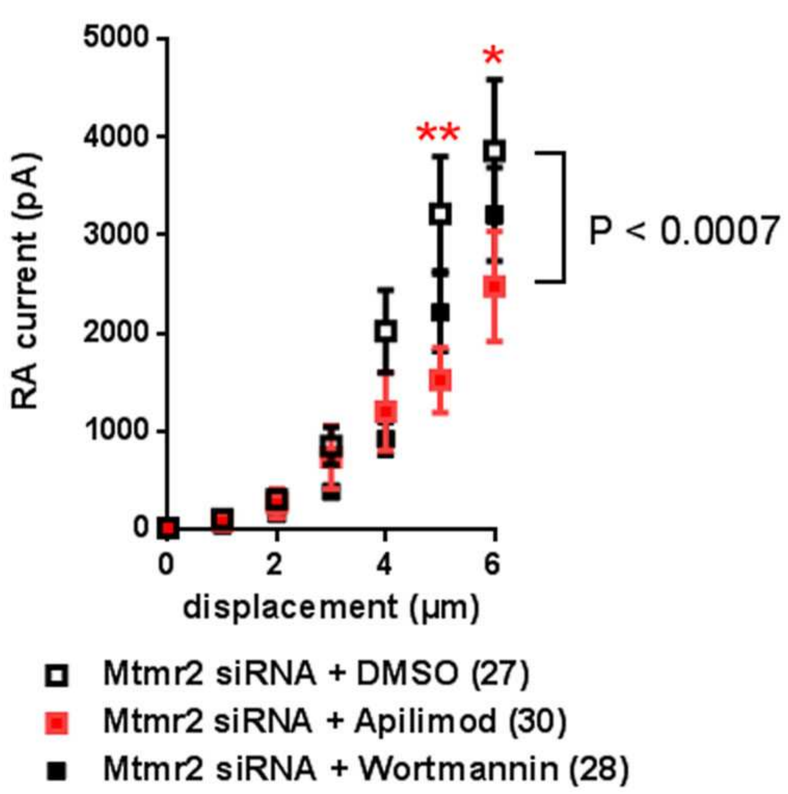

c

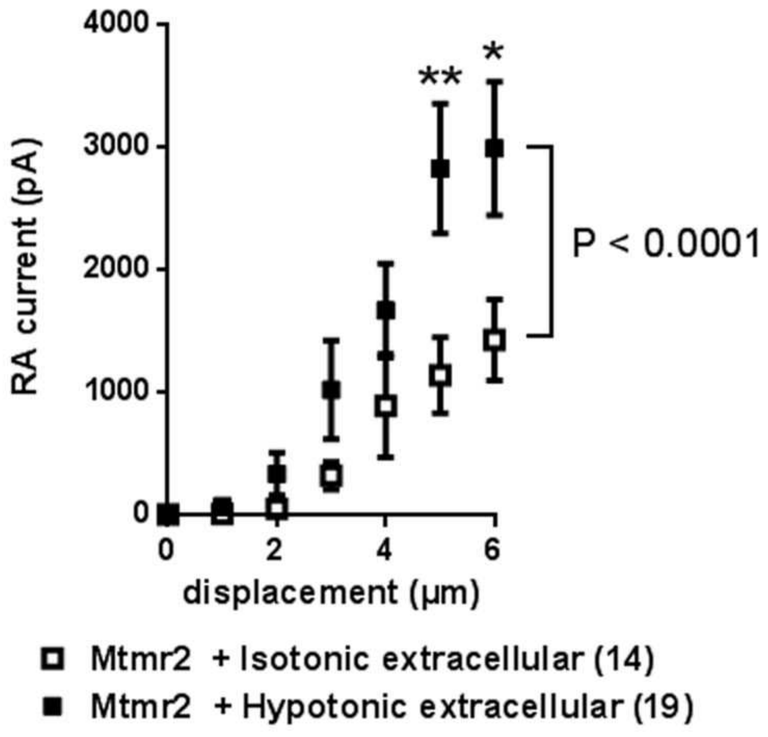

d

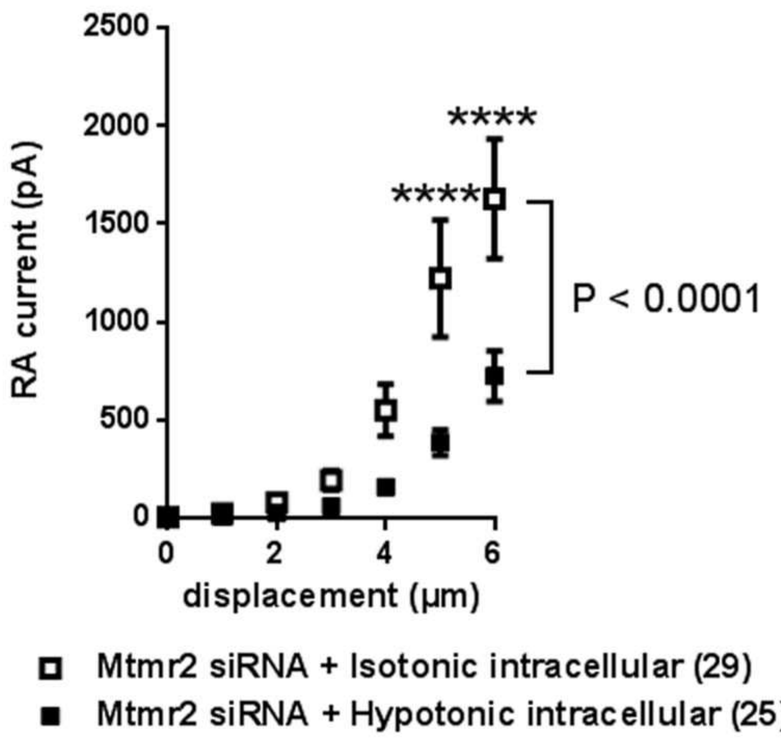

Figure 5

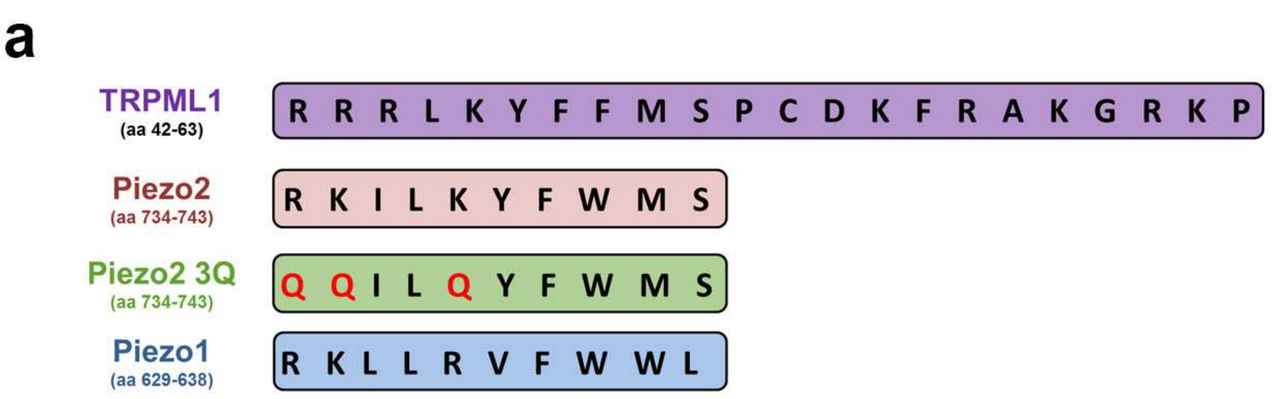
a
TRPML1
(aa 42-63)
R R R L K Y F F M S P C D K F R A K G R K P
Piezo2
(aa 734-743)
R K I L K Y F W M S
Piezo2 3Q
(aa 734-743)
Q Q I L Q Y F W M S
Piezo1
(aa 629-638)
R K L L R V F W W L

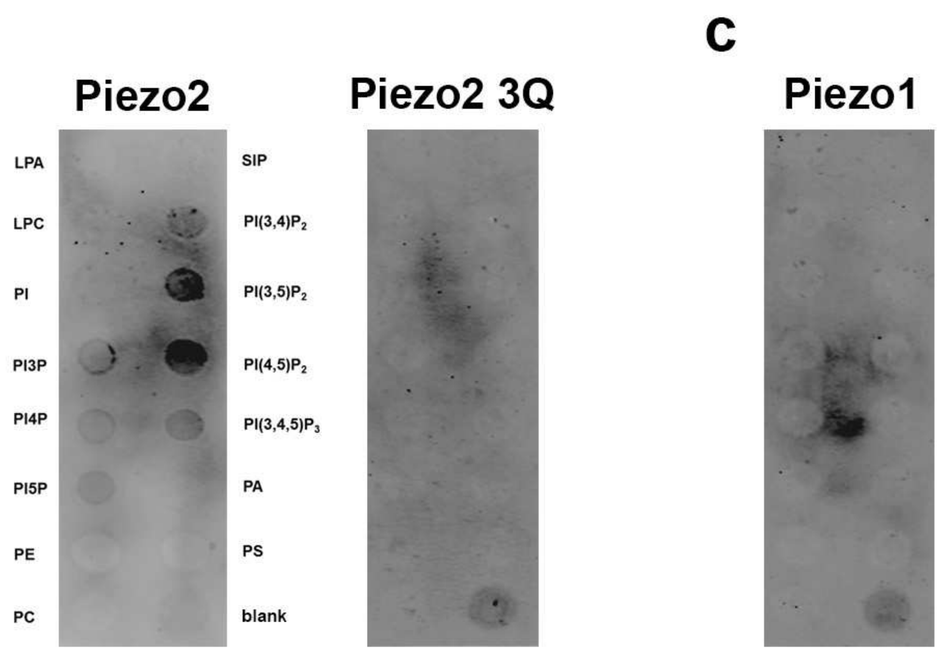
b
Piezo2
Piezo2 3Q
Piezo1
LPA
LPC
PI
PI3P
PI4P
PI5P
PE
PC
SIP
PI(3,4)P2
PI(3,5)P2
PI(4,5)P2
PI(3,4,5)P3
PA
PS
blank

c
Piezo2
Piezo2 3Q
Piezo1

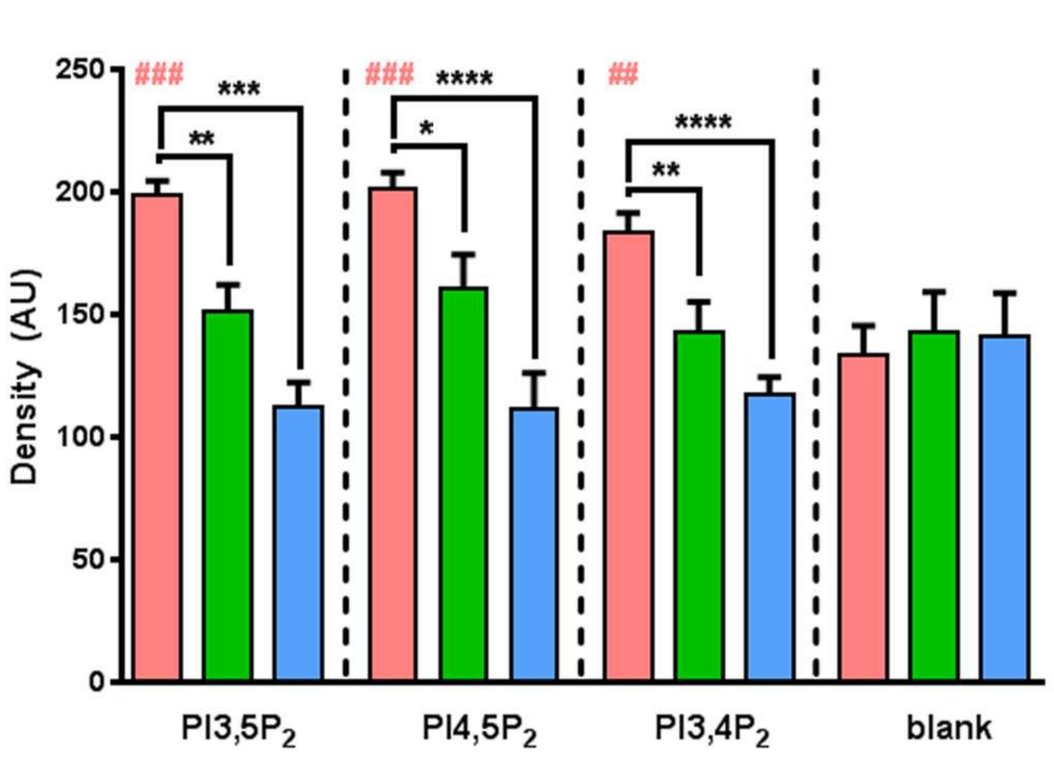
d
Density (AU)
250
200
150
100
50
0
###
**
***
###
*
****
##
**
****
PI3,5P2
PI4,5P2
PI3,4P2
blank

e
Piezo2 P1 mutant
RA current (pA)
2500
2000
1500
1000
500
0
0
2
4
6
displacement (µm)
P < 0.0119
Piezo2 P1 + mock (13)
Piezo2 P1 + Mtmr2 (10)

Figure 6

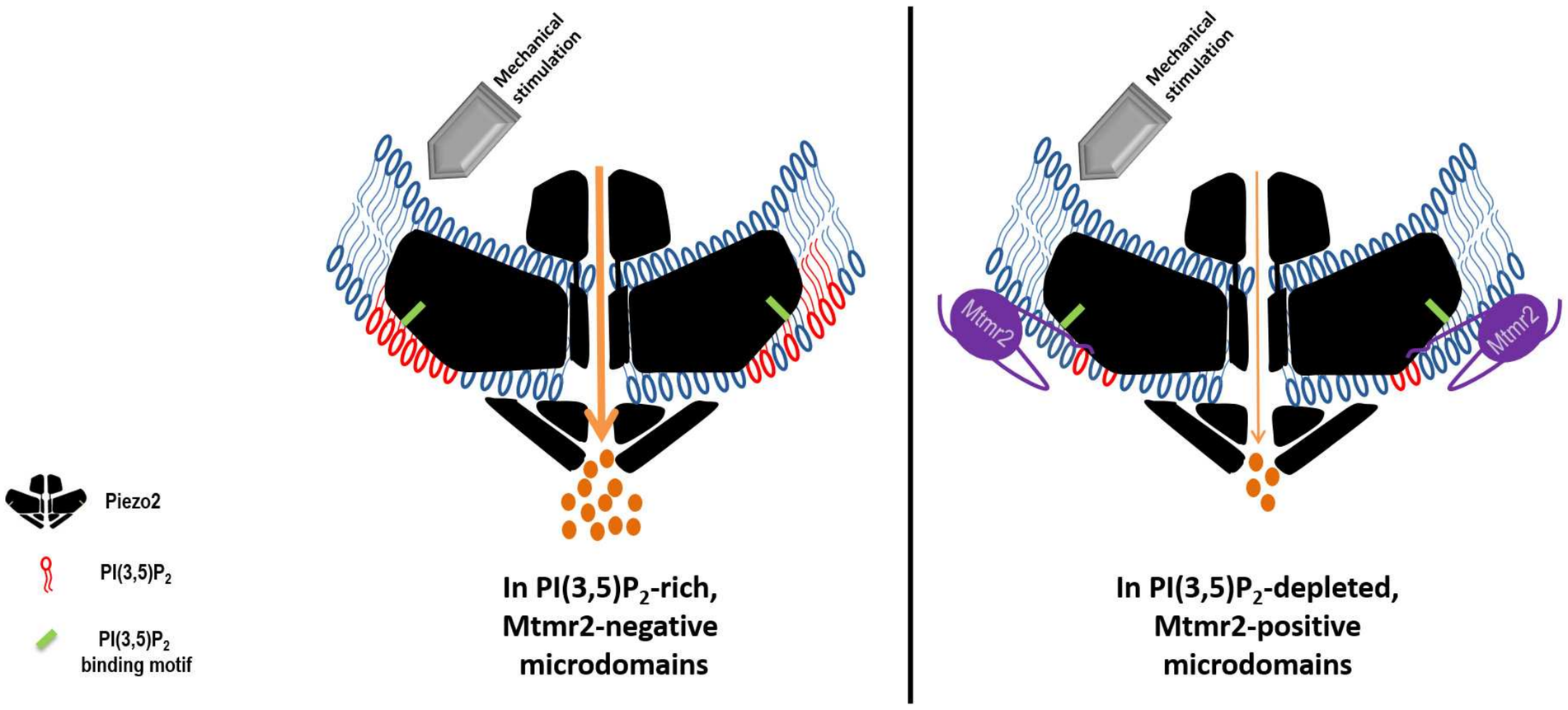
Mechanical stimulation
Mtmr2
Mtmr2
Piezo2
PI(3,5)P2
PI(3,5)P2 binding motif
In PI(3,5)P2-rich, Mtmr2-negative microdomains
In PI(3,5)P2-depleted, Mtmr2-positive microdomains

Figure 1-figure supplement 1

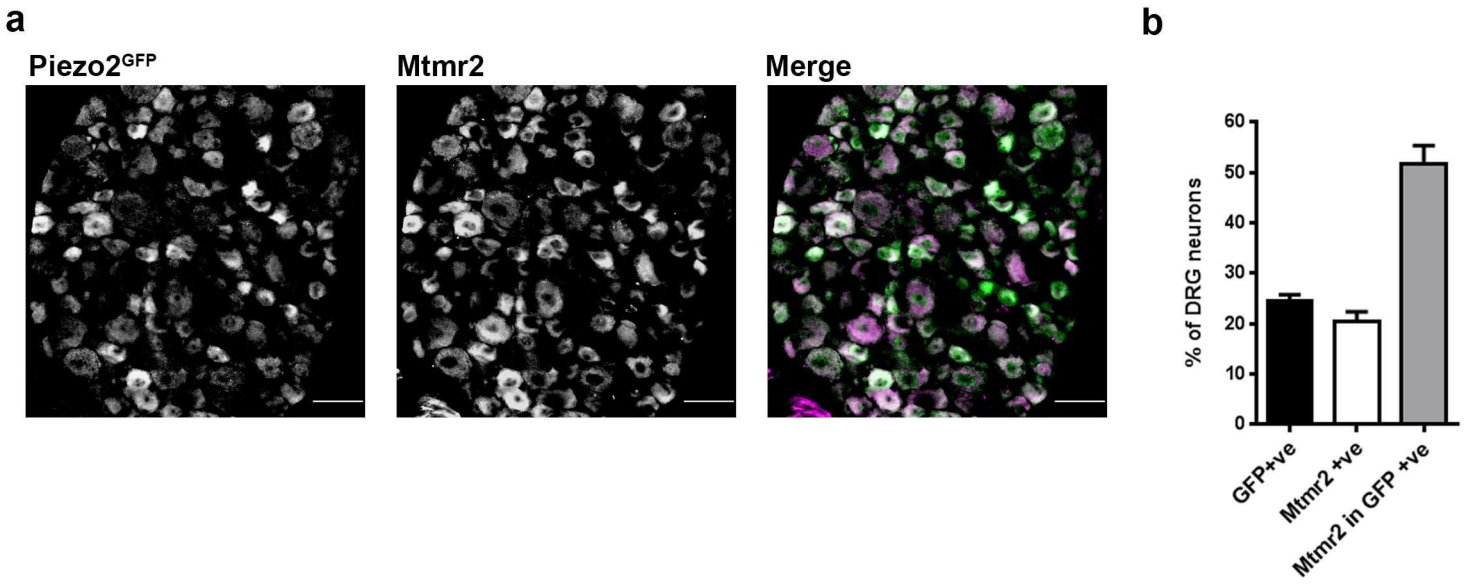

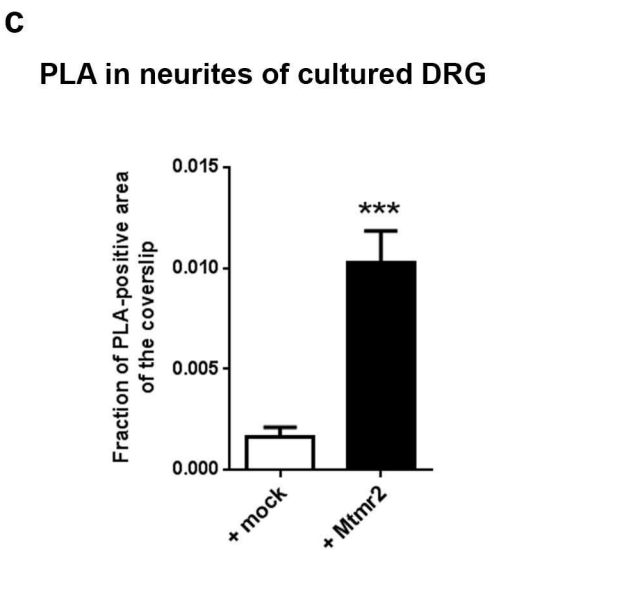

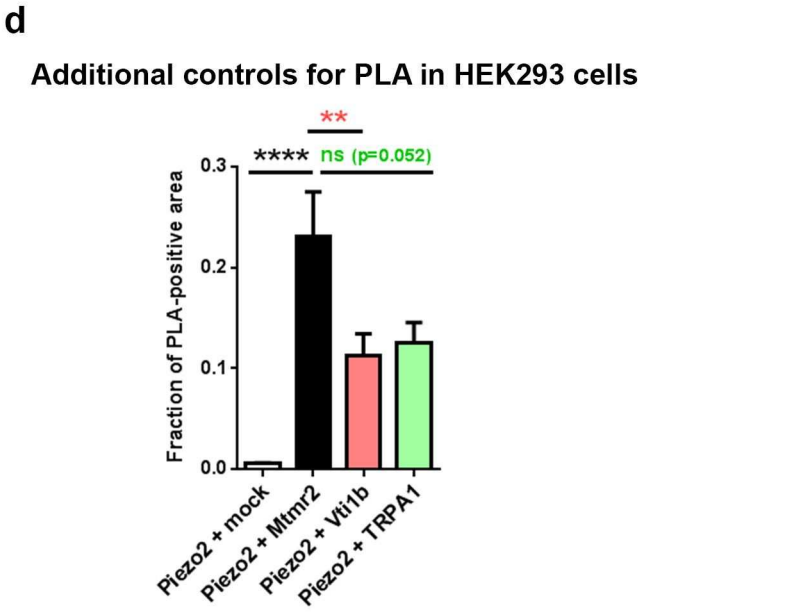

Figure 1-figure supplement 2

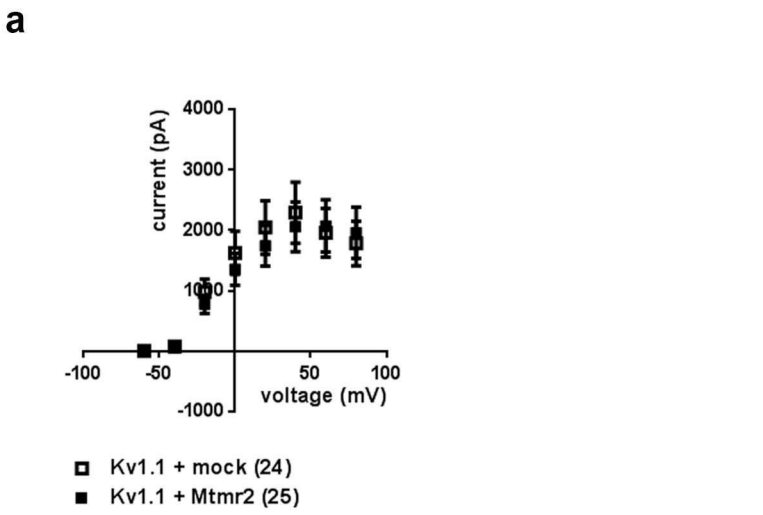

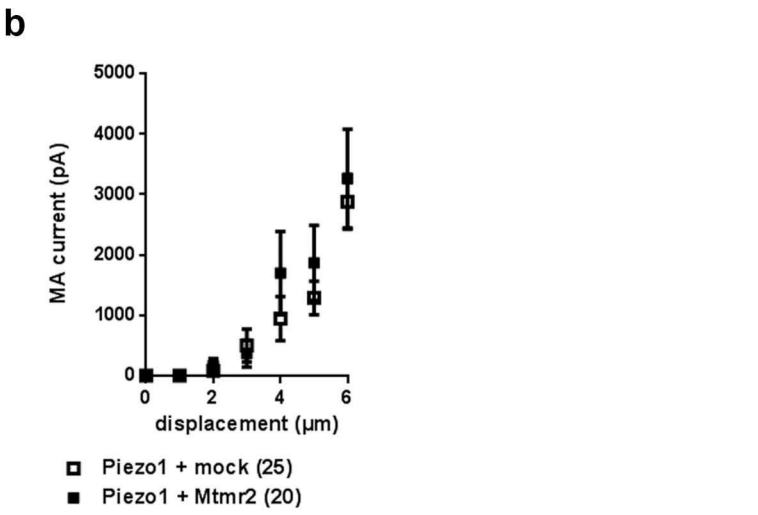

Figure 2-figure supplement 1

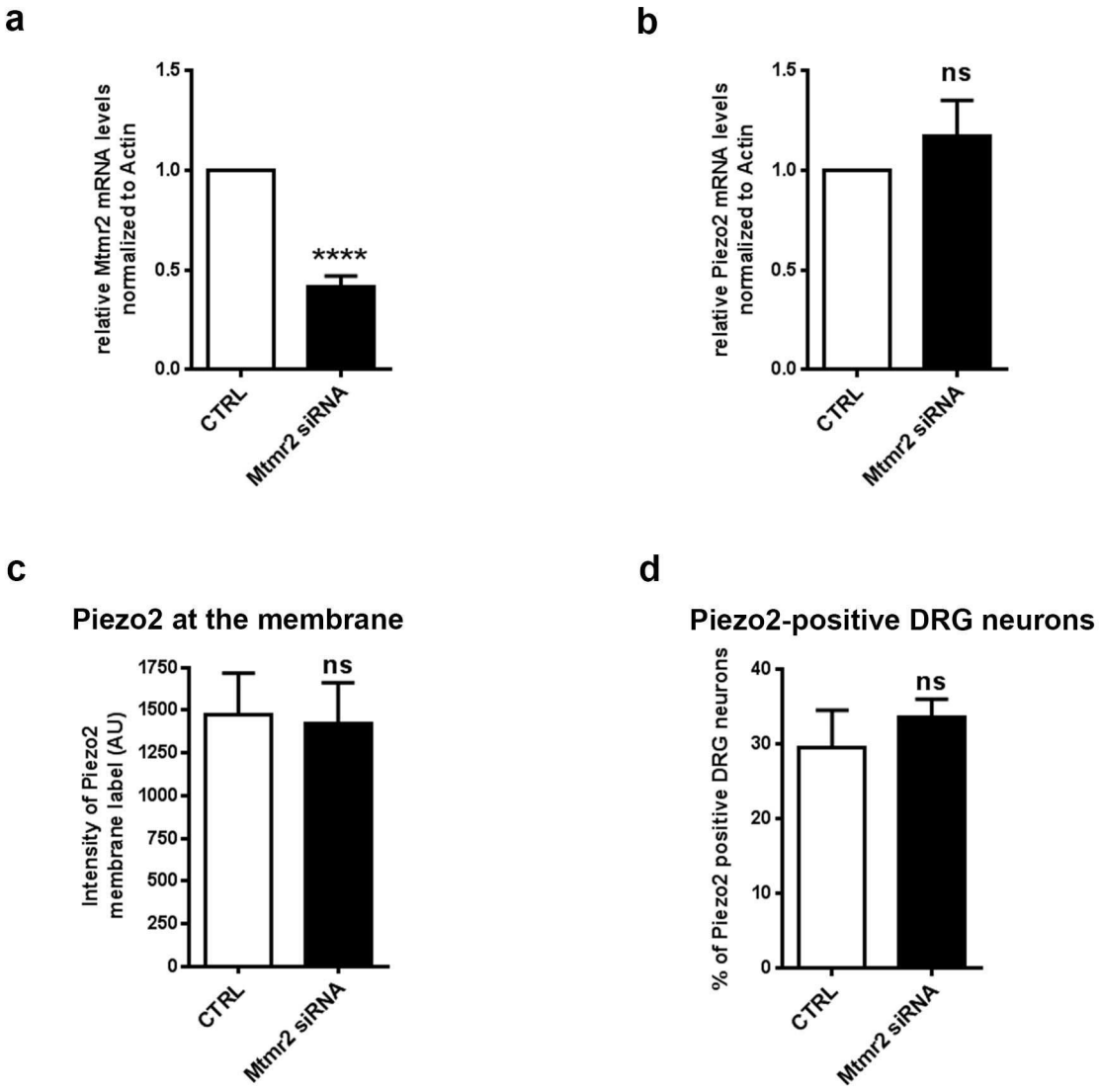

Figure 4-figure supplement 1

a

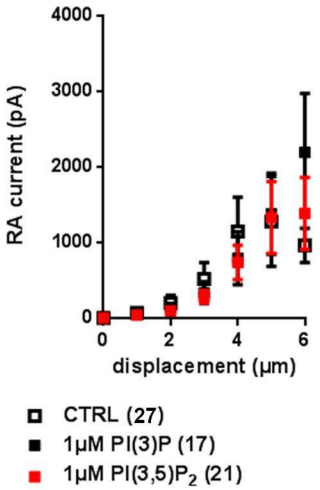

b

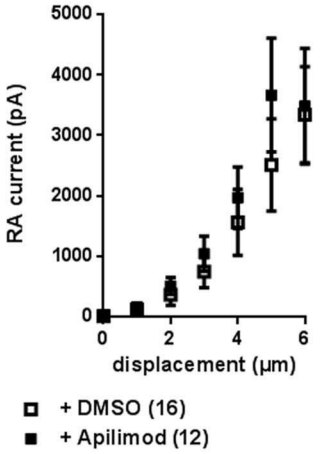

c

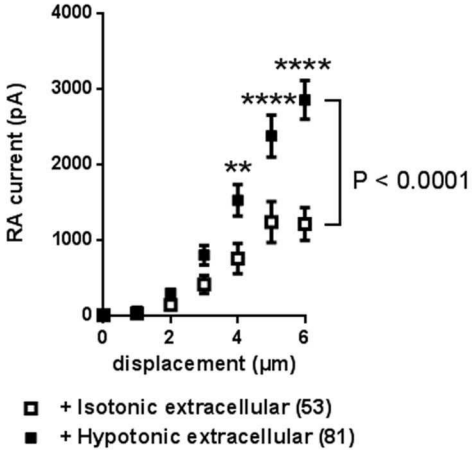

Figure 4-figure supplement 2

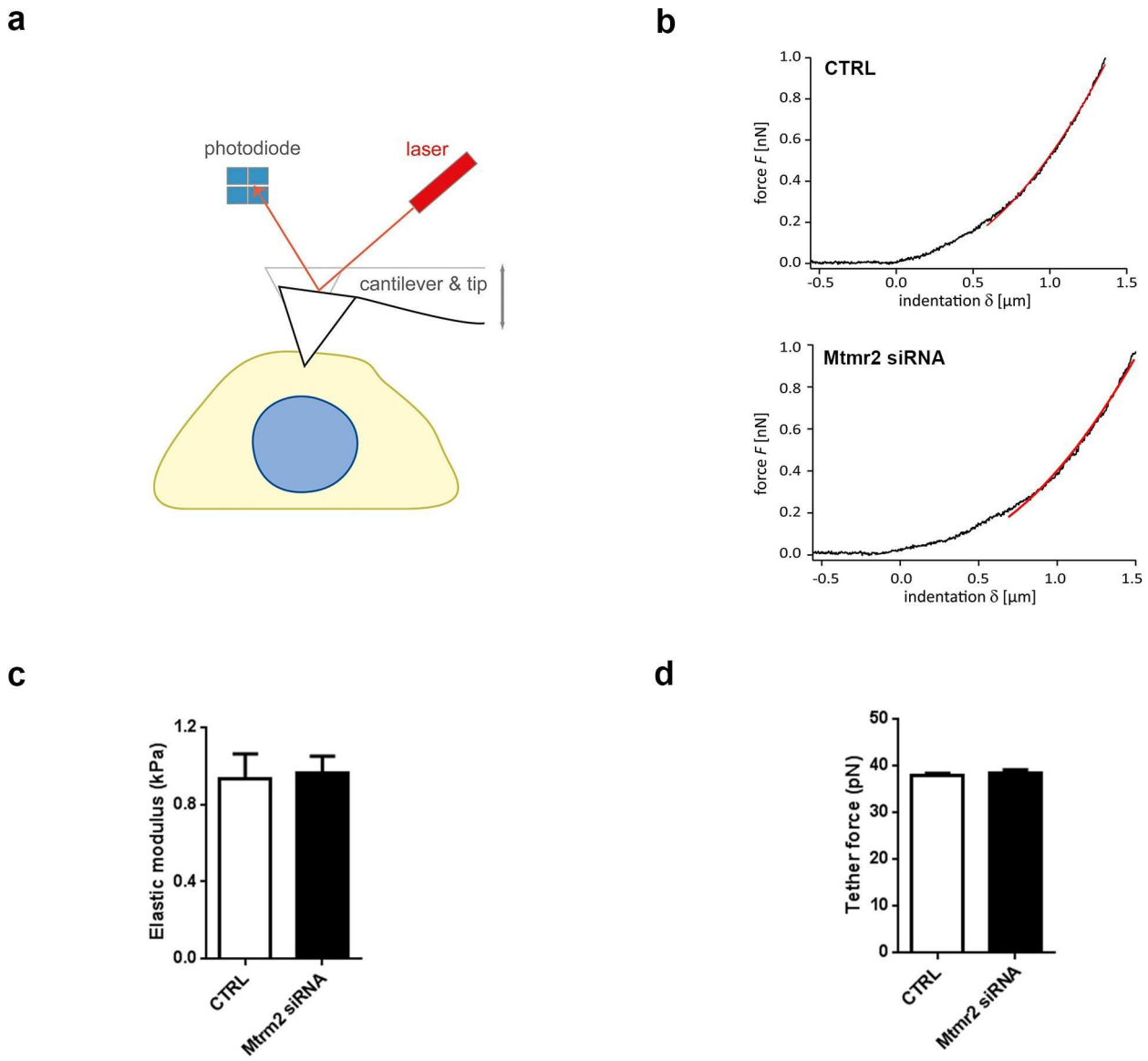

Figure 5-figure supplement 1